



HAL
open science

Future Directions for the Investigation of Surface-Bounded Exospheres in the Inner Solar System

Anna Milillo, Menelaos Sarantos, Cesare Grava, Diego Janches, Helmut Lammer, François Leblanc, Norbert Schorghofer, Peter Wurz, Benjamin D Teolis, Go Murakami

► **To cite this version:**

Anna Milillo, Menelaos Sarantos, Cesare Grava, Diego Janches, Helmut Lammer, et al.. Future Directions for the Investigation of Surface-Bounded Exospheres in the Inner Solar System. Space Science Reviews, 2023, 219, pp.49. 10.1007/s11214-023-00994-8 . insu-04209795

HAL Id: insu-04209795

<https://insu.hal.science/insu-04209795v1>

Submitted on 18 Sep 2023

HAL is a multi-disciplinary open access archive for the deposit and dissemination of scientific research documents, whether they are published or not. The documents may come from teaching and research institutions in France or abroad, or from public or private research centers.

L'archive ouverte pluridisciplinaire **HAL**, est destinée au dépôt et à la diffusion de documents scientifiques de niveau recherche, publiés ou non, émanant des établissements d'enseignement et de recherche français ou étrangers, des laboratoires publics ou privés.



Future Directions for the Investigation of Surface-Bounded Exospheres in the Inner Solar System

Anna Milillo¹ · Menelaos Sarantos² · Cesare Grava³ · Diego Janches² · Helmut Lammer⁴ · Francois Leblanc⁵ · Norbert Schorghofer⁶ · Peter Wurz⁷ · Benjamin D. Teolis³ · Go Murakami⁸

Received: 9 December 2022 / Accepted: 10 August 2023
© The Author(s) 2023

Abstract

Surface-bounded exospheres result from complex interactions between the planetary environment and the rocky body's surface. Different drivers including photons, ion, electrons, and the meteoroid populations impacting the surfaces of different bodies must be considered when investigating the generation of such an exosphere. Exospheric observations of different kinds of species, i.e., volatiles or refractories, alkali metals, or water group species, provide clues to the processes at work, to the drivers, to the surface properties, and to the release efficiencies. This information allows the investigation on how the bodies evolved and will evolve; moreover, it allows us to infer which processes are dominating in different environments. In this review we focus on unanswered questions and measurements needed to gain insights into surface release processes, drivers, and exosphere characterizations. Future opportunities offered by upcoming space missions, ground-based observations, and new directions for modelling are also discussed.

Keywords Surface-bounded exosphere · Mercury · Moon · Surface release processes

1 Introduction

Exospheres of airless bodies result from the complex interactions between the external agents and the surface, and the surface properties are crucial for determining the efficiencies of the various sources (Teolis et al. 2023). Different drivers in the environment must be considered when the exosphere generation mechanism is investigated. Particularly important are the ion (Wurz et al. 2022) and the meteoroid (Janches et al. 2021) populations impacting the surfaces of different bodies. In Fig. 1, a comparative scheme of the drivers and the released surface materials at Mercury and at the Moon is shown. In fact, exosphere observations of different class of species, i.e., volatiles or refractories (Grava et al. 2021a), alkali metals (Leblanc et al. 2022) or water group species (Schörghofer et al. 2021), can shed light on the release processes at work, not only on current solar system airless bodies,

Surface-Bounded Exospheres and Interactions in the Inner Solar System

Edited by Anna Milillo, Menelaos Sarantos, Benjamin D. Teolis, Go Murakami, Peter Wurz and Rudolf von Steiger

Extended author information available on the last page of the article

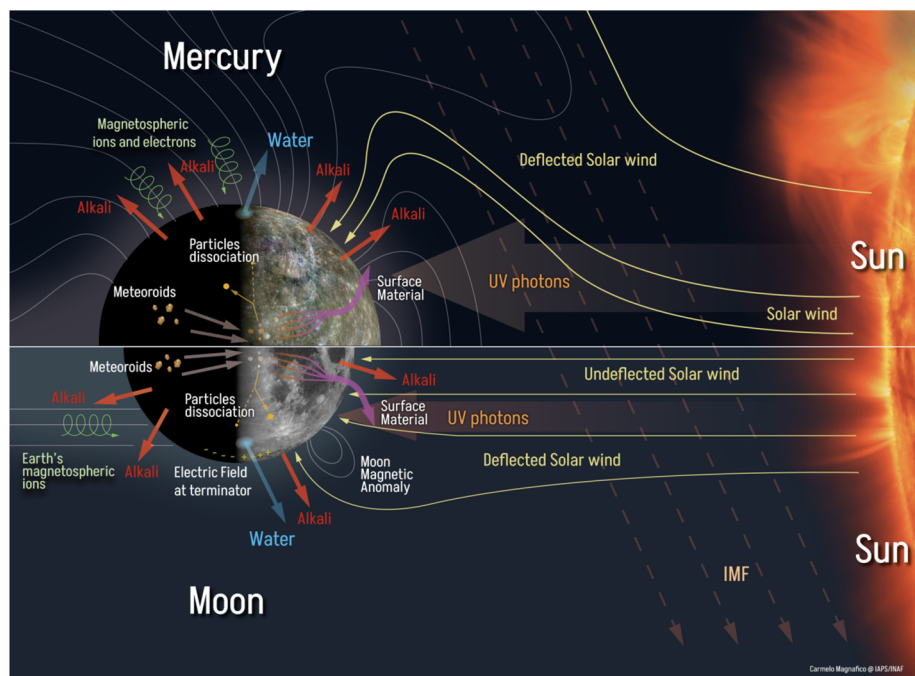


Fig. 1 Schematics of the processes at the two main airless bodies, i.e. Mercury and the Moon

but also on early solar system bodies such as planetary embryos and even close-in rocky exoplanets with magmatic surfaces (Lammer et al. 2022).

The most suitable and best studied examples of airless Solar system rocky bodies are the Moon and Mercury, but also asteroids and the two satellites of Mars are subject to similar interactions, with the big difference being the role of gravity (Schläppi et al. 2008; Plainaki et al. 2009; Nénon et al. 2019).

Already before the 1970s it was known that the Moon does not have a dense atmosphere (Hinton and Tausch 1964), but the first detection of Ar and He in the lunar exosphere was obtained during the Apollo missions (Hoffman et al. 1973; Hodges 1973a) (see Killen and Ip 1999 and references therein). In the following decade, Na and K have been observed using ground-based techniques (Potter and Morgan 1988). Lunar pickup have been observed near the Moon originally with the Suprathermal Ion Spectrometer (STICS) on the WIND spacecraft (Mall et al. 1998) and more recently measurements of Kaguya (Tanaka et al. 2009; Yokota et al. 2009, 2020), Chang'E-1 (Wang et al. 2011), the ARTEMIS mission (e.g.: Halekas et al. 2012; Poppe et al. 2012, Zhou et al. 2013), and the Lunar Atmospheric and Dust Environment Explorer (LADEE) mission (Halekas et al. 2015; Poppe 2016) confirmed the detections of H_2^+ , He^+ , C^+ , O^+ , Ne^+ , Na^+ , Al^+ , Si^+/CO^+ , K^+ , and 40Ar^+ (Poppe et al. 2022). At Mercury, only an upper limit for neutral oxygen has been obtained (Shemansky 1988). In both cases, it is possible that the oxygen is in molecular form in the exosphere. In the meanwhile other species have been identified in the exosphere: CH_4 , Ne, Rn, and $\text{OH}/\text{H}_2\text{O}$ (Stern 1999; Benna et al. 2015; Hodges 2016).

Lunar noble gases (helium, argon, and neon) were amongst the first exospheric species measured by mass spectrometry during the Apollo 17 mission (Hoffman et al. 1973). Those detections have been confirmed by the Lunar Atmosphere and Dust Environment Explorer

(Benna et al. 2015; Hodges and Mahaffy 2016) and Chandrayaan-1 (e.g., Dhanya et al. 2021). These gases are exemplary species for studying the gas-regolith interaction because they indicate various degrees of gas-surface bonding. The neon density at the surface increases from dusk to dawn as the regolith surface cools off, exhibiting the behaviour expected for a non-condensable species. In fact, for such species, where the gas atoms do not lose sufficient energy upon impact with the surface, or even when they do, the bond is so weak that they immediately (within micro to nanoseconds) are emitted again, the exospheric density at the surface, n , is expected to be inversely related to the surface temperature, T : $n \sim T^{-5/2}$ (Hodges and Johnson 1968). Helium is also a gas that does not freeze out at the coldest night-time temperatures, but exhibits a pre-dawn peak and a decrease towards dawn, deviating from the predicted behavior for non-condensable species because of the larger ballistic range for these light atoms. And last, argon density decreases from dusk to dawn and then increases at dawn, which is the behavior consistent with a condensable species.

The measurements of these and other volatile species, like methane (Hodges 2016) and molecular hydrogen (Stern et al. 2013), raised questions about precisely how gases lose energy when in contact with regolith. For example, there has been a long-standing debate on whether helium atoms in the lunar exosphere should be thermalized with the surface. This issue has been resolved only recently, with spectroscopic observations confirming the thermalization of lunar exospheric helium (Grava et al. 2021b). As another example, the adsorbable nature of argon from measurements of the LACE (Lunar Atmosphere Composition Experiment) mass spectrometer deployed on the lunar surface by the Apollo 17 mission was not expected for a noble gas. Exosphere models require the adoption of unexpectedly high values of the activation energy for desorption of argon-40 (e.g., Bernatowicz and Podosek 1991; Hodges and Mahaffy 2016; Hodges 2016) to match the measurements. This was initially attributed to the cleanliness of the pristine lunar regolith. More recently, Kegerreis et al. (2017) and Sarantos and Tsavachidis (2020, 2021) noted the role of regolith microstructure in prolonging the ability to temporarily retain argon and other gases by Knudsen diffusion within the first mm of regolith. This should also apply to deeper and long-term sequestration of water (Schörghofer 2022) and species of similar volatility. About 30% of the ejected argon atoms are ultimately adsorbed in the Permanently Shadowed Regions (PSR) near the lunar poles (Grava et al. 2015), and another fraction ends up in seasonal polar shadows from which they can be re-emitted every half year, creating seasons (Kegerreis et al. 2017; Hodges 2018). In fact, the polar regions of the Moon are expected to contain a vast repository of volatile gases trapped in the regolith. These atoms and molecules were either transported to the poles via exospheric ballistic hopping, and/or they were synthesized from simpler atomic constituents which landed on grains that act as catalysts.

The source of volatile gases is the lunar interior as well as implanted solar wind. At least some of the helium, ranging by different estimates between 10% (Hodges 1975) to 15–20% (Benna et al. 2015; Grava et al. 2021b) and even up to 40% (Hurley et al. 2016), appears to be effusing from the interior the surface originating from the decay of radiogenic elements. LADEE measurements discovered an enhancement in exosphere density above western maria and Oceanus Procellarum (Benna et al. 2015) that is likely related to the enhanced abundance of ^{40}K at those locations (Kegerreis et al. 2017). Selenographic variations have been demonstrated in other gases whose distribution on the ground is non-uniform such as potassium (Colaprete et al. 2016; Rosborough et al. 2019).

The first observation of Mercury's exosphere has been obtained by Mariner 10, during its fly-bys of Mercury. The UVS spectrometer revealed H, He and an upper limit of atomic oxygen as constituents in its exosphere (Broadfoot et al. 1974, 1976).

Mariner 10 fly-bys revealed the existence of a weak internal global magnetic field (Ness et al. 1975, 1976) with the dipole axis approximately aligned with its spin axis. This dipole

field is strong enough to maintain a small magnetosphere populated with plasma originating from the solar wind and from the planet's exosphere. This observation implies a more complex interaction of the Mercury with the solar wind and Interplanetary Magnetic Field (IMF) through its small magnetosphere.

Since the second half of 1980s up to present day, Earth-based observations revealed important features about the exosphere of Mercury (see reviews by Killen et al. 2007; Leblanc et al. 2022), but they are limited to species observable through Earth's atmosphere, which are Na, K, and Ca (e.g.: Potter and Morgan 1985, 1986; Bida et al. 2000). It is quite challenging to observe Mercury with telescopes operated during night, because of its vicinity to the Sun; Mercury is visible only for a few hours before sunrise or after sunset, so it is difficult to investigate the variability of the exosphere. Since the 1990s advanced technologies allowed much-prolonged day-time observations with Solar telescopes, thus allowing studies of short time variabilities (Mangano et al. 2015; Massetti et al. 2017; Leblanc et al. 2022). The main observables in the ground-based observations are the D1 and D2 emission lines of the Na exosphere with its variable distribution sometime spread to the whole sunlit hemisphere, sometime with two peaks in Northward and Southward hemispheres (e.g.: Potter and Morgan 1990; Potter et al. 1999). The ground-based observations of the D2 line emission of K show similar distributions (Potter and Morgan 1986, 1997). This variability and increase in emission intensity just below regions (cusps) where the solar wind is expected to enter and impact to the surface, made it clear that there is a correlation between alkali distribution and ion impact onto the surface (Killen et al. 2001). The strict relation of Na exosphere variability with plasma impact onto the surface is supported by the lucky observation of Na ground-based observation during an interplanetary Coronal Mass Ejection (iCME) arrival at Mercury registered by MESSENGER on 20 September 2012 (Orsini et al. 2018). In fact, during this observation the Na exosphere showed a distribution that changed when the dense iCME plasma likely compressed the dayside magnetosphere.

Despite this evidence, there are still many unexplained features that require further observations, laboratory measurements and modelling that will be described in the next sections. In fact, the ion sputtering process, as studied in laboratory experiments, has a low efficiency for solar wind ions on rocky regolith, and cannot justify the observed high column densities of Na (up to 10^{11} cm²) with an altitude profile consistent with temperatures of about 1200 K typical of Photon Stimulated Desorption (PSD) release process (Cassidy et al. 2015; Wurz et al. 2022).

Another specific feature of the Na exosphere is the formation of an anti-sunward tail that is strongly variable along Mercury's orbit (e.g: Potter et al. 2002a,b; Potter and Killen 2008), clearly proportional to the solar radiation pressure. This Na tail is a visual display of the Na loss rate from the planet (Schmidt et al. 2012) comparable to other exospheric species losses (Wurz et al. 2019). Given this loss, the investigation of Na source-sink balance is still an open question. In fact, it is still not clear how the Na content at Mercury's surface evolves in time.

The observations of MESSENGER during flybys and during the whole mission confirmed the presence of an internal magnetic dipole moment of 190 nT R_M^3 and found that the dipole is offset northward by about 0.2 R_M . (Anderson et al. 2011). Furthermore, MESSENGER MAG and FIPS observations depicted a really dynamic magnetosphere, with a strong coupling with the external solar wind conditions and a high reconnection rate that produces a frequent and efficient solar wind entry and circulation inside the magnetosphere (Slavin et al. 2021). For the first time MESSENGER observed planetary heavy ions in the magnetosphere: Ca⁺ by Mercury Atmospheric and Surface Composition Spectrometer (MASCS) and He⁺, water groups and Na⁺-Mg⁺-Si⁺ groups by FIPS (Zurbuchen et al. 2011; Raines

et al. 2013). The heavy ion populations in the magnetosphere implies surface release mechanisms directly in ionized state or an efficient photoionization of the exospheric components (Wurz et al. 2019). On the other hand, if these heavy ions impact onto the surface at day and night sides, they may contribute to produce a second-generation exosphere (e.g.: Delcourt et al. 2003; Milillo et al. 2005, 2020).

MASCS UV and Vis spectrometer regularly observed Na (mainly in the low latitudes regions), Ca and, for the first time, Mg atoms in the exosphere (McClintock et al. 2008; Killen et al. 2007). And later Bida and Killen (2017) detected from HIRES ground-based observations traces of the minor species Al and Fe.

The MESSENGER Na observations analysed together with the ground-based observations, showed that superimposed on the short-term variability there is a long-term variability of Na exosphere along the orbit. The global Na density as well as asymmetries in local time and latitudes distributions have a clear recurrence along Mercury's year (Potter et al. 2006; Cassidy et al. 2015; Milillo et al. 2021; Leblanc et al. 2022). The science community is still debating on a global scenario able to fully explain these behaviours.

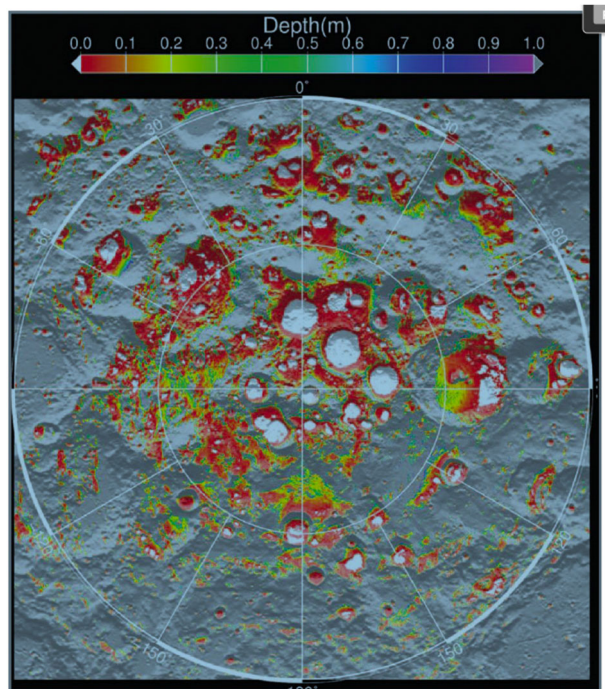
Finally, MESSENGER detected Mn and Al in Mercury's exosphere (Vervack et al. 2016), the latter was previously observed with low signal/noise ratio by ground-based observations by Bida and Killen (2016). Unexpectedly for a highly oxidated surface (Wurz et al. 2010), the presence of atomic oxygen in the exosphere was still not confirmed, thus a debate on where it is and in which form is still ongoing.

The MESSENGER observations showed a clear dichotomy in the exospheres of different kind of species; in fact, while moderately volatile component, like alkali, i.e. Na and K, distributions have a long term variability along Mercury's orbit and a short term variability especially at high latitudes, the refractory component like Ca and Mg have predominantly a source in the ram hemisphere (in direction of the planet velocity) (Burger et al. 2014), where most of the meteoroids impacts the surface due to the relative velocity of Mercury and the dust disk particles (Pokorný et al. 2018; Janches et al. 2021). The correlation with the expected meteoroid impacts is proved also by the Ca enhancement in the exosphere when Mercury crosses the trajectory of the comet 2P/Encke dust stream (Killen and Hahn 2015). Thus, for these species a Micrometeoroid Impact Vaporization (MIV) is the expected primary generation process. Nevertheless, the high scale height of these components, firstly spotted from the challenging Ca ground-based observation by Bida et al. (2000) and confirmed and quantified (corresponding to a characteristic temperature above 20,000 K, inferred from the scale height) by MESSENGER/MASCS measurements is not easily explainable by the even more energetic surface release processes, like ion sputtering or MIV. This mismatch between the expected and observed distribution of refractory species, opens debate on the possible multiple complex processes able to energize the particles after the release from the surface. The release of molecules (e.g. oxides), which are subsequently dissociated into atoms, could be the pathway for explaining the observed high characteristic energy of some refractory species (Killen 2016; Grava et al. 2021a).

It is likely that a complex mechanism acting in the solar wind - magnetosphere - surface interaction should be invoked to fully explain the Na distributions at Mercury. Given that the whole surface material is released via MIV, the role of this process in the release of different species is also an open point. Any progress on this subject will be dependent on a better understanding on what controls different types of diffusion. The development of models of volatile diffusion coupled with exospheric 3D models and dedicated laboratory experiments are of great importance for the interpretations of the observations.

Despite the crucial role of the water in astrobiology studies, the relative and absolute magnitudes of sources of members of the water group (H₂O, OH, ...) on Mercury and

Fig. 2 Near surface ice stability is modelled to be possible over vastly larger areas than strict PSR (white areas). The coloured regions represent different depths to reach ice stability in the top 1 meter of regolith. (From Paige et al. 2010)



on the Moon remain uncertain. Water released into the exosphere can potentially migrate globally, and become trapped at the cold traps at PSR (Watson et al. 1961; Paige et al. 1992; Schörghofer et al. 2021) (Fig. 2). Slade et al. (1992) observed radar-bright spots at the northern pole at Mercury with Arecibo and Goldstone radar telescopes, later confirmed by MESSENGER observations to be water ice (Chabot et al. 2018). Evidence for cold trapped ice on the Moon comes from neutron spectroscopy (Feldman et al. 1998; Lawrence 2017), the LCROSS impact experiment (Colaprete et al. 2010), UV albedo ratios (Hayne et al. 2015), and near-infrared spectroscopy (Li et al. 2018); see Lucey et al. (2022) for a more detailed review. For analogy, bright spots inside cold traps have been identified also on Ceres by images from the Dawn spacecraft and are likely also made up of ice (Platz et al. 2017). At this point it remains unclear whether this cold-trapped ice was delivered by an exosphere or deposited during rare events that sporadically create temporary atmospheres. It is also possible that the dominant formation and accumulation mechanism may vary from body to body and with distance from the Sun.

Complementary to the exospheric observations are laboratory experiments for investigating the planetary analogues interacting with different drivers, like ions, electrons and UV photons. In Sect. 2, some open points in the surface release processes and the way the next studies will try to answer are described.

For a better understanding of the interaction between the surface and the external environment, we need to characterize the drivers, i.e., impacting plasma, dust distribution, solar UV irradiation of at the surface, as well as the generated exosphere. In Sect. 3, some observations that will help to characterize the drivers thanks to the near-future missions around the Moon and Mercury are described and suggested. In Sect. 4, we describe the open questions in the investigation of the composition, dynamics, sources and loss rates of the exosphere.

Coordinated space and ground-based observations are suggested and expected outcomes are depicted.

Finally, for a deep and global understanding of the exospheric environment we need models for the generation and circulation of the exosphere. Comparison of simulated exospheres with observations of different species will be an essential tool for interpreting the results, for validating theories of exospheric generation and eventually for showing where there are knowledge gaps. In Sect. 5, a short review of more advanced models for airless bodies is given and the direction of further model improvements are suggested. Summary of the expected results of the study of airless bodies' interaction with their parent star and next mission outcomes are described in the final Sect. 6.

2 Open Points on Surface Release and Space Weathering Processes

The observations of the Hermean and lunar exospheres are on spatial scales commensurate with the dimensions of the object, from ~ 100 km size features (like the sputter contribution at the magnetospheric cusps), to global exospheres (e.g., the He exosphere), to extended tails of Na of several, even 1000 planetary radii (Potter et al. 2002a,b; Schmidt et al. 2012). The external drivers causing the population of these exospheres are varied in their spatial and temporal extent (Wurz et al. 2022).

However, for the quantitative understanding of the release processes also the micro-physics has to be understood very well. Particle release processes act on very small spatial scales, all the way down to the atomic scale on the surface. It is important to consider in the analysis the actual material, which is fine grained regolith with highly structured grains resulting from the micro-meteorite gardening over millions of years. Moreover, the very surface of these grains is chemically and physically altered by processes of space weathering (ion impact, solar irradiation, ...).

Laboratory measurements of thermal desorption rates and residence time on grains are needed to better understand the surface-exosphere relationship and thus explain the dependence of volatiles' exospheres with local time and solar zenith angle. Experiments that derive yields, cross sections, and threshold energy for PSD and electron-stimulated desorption, which are major source processes for some volatiles, would ultimately need improved simulations of surface-bounded exospheres. Desired simulations are the study of diffusion of volatiles on soil grains, the effect of topography (both at the micro-scale, such as shadow from grains, and at the macro-scale, such as mountains and craters) on the exosphere, and the destruction of deposits of frozen volatiles in PSRs from micrometeoroid bombardment and photolysis from Lyman-alpha photons and cosmic rays.

Despite many research studies are available on processes of interaction of ions, electrons, and photons with the surfaces and their effects on surface modification and particle release, the grains of rocky regolith on planetary surfaces often do not have the same properties as surface analogues investigated in laboratory studies. Generally, the theoretical modelling of surface physics processes has to rely on simple surfaces, which are far away from realistic surfaces to be encountered on planetology. Therefore, we should also explore more complicated surfaces to provide suitable information for studies of particle release in planetary systems. A study accounting for the structured regolith surface was done by Szabo et al. (2022a, 2022b).

In the following sub-sections, a brief overview of surface release processes is provided. More detailed descriptions can be found in Wurz et al. (2022).

2.1 Thermal Desorption

Thermal desorption of solids is well understood for pure species, e.g., the sublimation of water (e.g. Fray and Schmitt 2009). The situation becomes more complicated for mixtures, e.g., CO₂ in water ice, where the sublimation fluxes for H₂O and CO₂ as a function of temperature will depend on the mixing ratio. The most complicated case are adsorbed layers, at the level of monolayer or fractions of it, on surfaces. Here, the examples are Na atoms on the mineral surface. Clearly, the sublimation flux of pure Na would give too high release fluxes. The binding energy of Na to the mineral substrate (e.g. the regolith grains) will be a function of the mineral itself, the structure of the surface (ideally flat, but in reality highly structured), the association of the Na atoms (i.e., localized Na islands or individual Na atoms scattered of the surface), and the exact location of the Na atoms on surface features. For example, the activation energy for release from the surfaces is lowest when the Na atom is on a piece of flat surface, higher when located at a step, and even higher in the corner of a structure. Thus, the microscopic structure of the surface is important. Activation energies for thermal desorption for structured surfaces have to be studied in the laboratory. Recent laboratory experiments, in fact, will focus on sticking coefficients and residence times of Na atoms on the surface, which is important information for the circulation of Na between the exosphere and the surface (Sarantos and Tsavachidis 2021).

2.2 Sputtering by Ion Impact

Sputtering by ion impact is a well-studied process in surface science for many decades since sputtering is used for a range of industrial and analytical applications. However, the sample studies are often not representative of actual surfaces encountered in planetary science. Studies of sputtering from mineral grains, considering fractured surfaces, with significant porosity are mostly missing. Anyway, the theoretical background for understanding the effect of porosity on sputtering is currently developed (Szabo et al. 2022a, 2022b). Moreover, the top surface of 50–100 nm of the regolith grains are space weathered (Pieters and Noble 2016), resulting in different composition and crystal structure, which strongly will affect the sputter yields. Moving from the microscopic to the macroscopic scale, there is a range of minerals present in the regolith, given by the mix of grains in the surface, which will have different sputter yields for the species. Combining these varieties into macroscopic sputter yields for provinces on the lunar or Hermean surface still has not been done. For example, several lunar magnetic anomalies are spatially correlated with surface regions of high albedo of the lunar regolith, known as “lunar swirls” (e.g. Denevi et al. 2014). A possible explanation is that the deflection of solar wind protons in highly magnetized regions prevents or reduces space weathering and darkening of soils (Hood and Williams 1989). This idea is also supported by the OH depletion that is the signature of reduced proton implanting onto the surface (Schaible and Baragiola 2014). The ion impact at the edge of the mini-magnetosphere above the magnetic anomalies, on the contrary, will cause enhanced diffusion inside the regolith grains, ion sputtering, back-scattering of ions and neutral atoms (see also Sect. 3)

The generation of hydroxyl and then molecular water by the interaction of solar wind protons with silicate grains is crucial to our understanding of water formation on large airless bodies (Schörghofer et al. 2021). The efficiency of this process needs to be quantified in laboratory experiments for a variety of compositions and surface properties (ideally with lunar samples).

2.3 Photon Stimulated Desorption

PSD is a process that operates on the atomic scale. A UV photon is absorbed by atoms localized on the surface which may result in the electronic excitation of an atom residing on the surface, e.g. Na, rendering into an anti-binding state causing release of this atom. Although Desorption Induced by Electronic Transitions (DIET), by photons and electrons, has been studied in the surface science community for many decades (see Wurz et al. 2022 and references therein), the particular surfaces relevant for planetology have been studied only for very few cases. Studies on the dependence of the release of Na, K, and others from photon wavelength and the corresponding cross-sections of the interaction are mostly missing for regolith grains. Also, the energetics, i.e., the energy distributions of the released particles are not well studied, and often thermal distributions are assumed in the modelling and analysis of observations even though this process is a DIET process and not a thermal process.

2.4 Electron Stimulated Desorption

Electron stimulated desorption (ESD) is a surface release process comparable to the PSD at microscales (see Wurz et al. 2022 and references therein) even if the driver has a different nature and distribution. Since both electrons (in the energy range 15-hundreds eV) and UV photons produce the same electronic excitation on surface atoms, the velocity distributions of the released particles are the same. The cross sections of the processes are quite similar, but since the electron fluxes are generally much lower than the photon fluxes this process is generally masked by PSD in the dayside of the bodies. The efficiency of this process at Mercury and Moon could be investigated in the nightside surface.

2.5 Micrometeoroid Impact Vaporization

Most of the dust particles hitting the surface of Mercury and the Moon are meteoroids, with sizes in the range of typically 1 to 100 μm . Thus, the affected volume at the impact size is of similar dimension, a microscopic process on the surface. The high speed of the impacting dust particles gives rise to an impact plume, releasing material from the surface. This material is broken up pieces from the surface, atoms, molecules, ions. The temperature of the shock-induced cloud just after impact (the first 100 ns) was estimated to be between 15,000 K and 27,000 K. The temperature and pressure quickly decrease during adiabatic expansion of the cloud reaching a quenching temperature, typically 2000–5000 K. During the rapid expansion of the plume, non-equilibrium processes take place resulting also in the formation of molecules (Berezhnoy 2013, 2018). Thus, the input to the exosphere is not just atoms, but also molecules. For the latter their internal temperature (rotation and vibration) influences how long they will survive in the exosphere before they separate into their atomic constituents. Little information is available about the thermodynamic conditions in such plumes, and laboratory studies with dust impacts at the relevant impact speeds could be performed for a combination of relevant impactor and surface materials (Cintala 1992).

Another area which requires further work for MIV process description concerns laboratory experiments. Experimental results from Koschny and Grün (2001) predict lunar dust cloud density values higher by four orders of magnitude than those inferred from LDEX measurements (Pokorný et al. 2019). This discrepancy could be partially due to the very low velocity impacts (1–12 km/s) experimented on ice-rich surfaces for estimating the yield. Clearly experiments better matched experimental conditions are needed to advance in this area.

3 Open Points on the Characterization of the Drivers (Meteoroids, Ions and Electrons)

As mentioned in the previous section, the external drivers causing the exosphere generation are varied in their spatial and temporal extent (Wurz et al. 2022).

The Sun illuminates the entire dayside, but because of the irradiation dependence on the solar zenith angle there is a longitudinal and latitudinal variation of its effect on the thermal release and release via photon stimulated desorption. The ion sputtering is driven by the solar wind ions and magnetospheric ions hitting the surface. For Mercury, the ion bombardment displacement at the surface depends on the configuration of the magnetosphere, which adjusts itself to the solar wind plasma and magnetic field parameters on short time scales. The global situation is simpler for the Moon, spending most of its time in the solar wind, but there is also the passage through the terrestrial magnetosphere which sends different plasma populations to the lunar surface (Kallio et al. 2019). At some locations on the lunar surface there are magnetic anomalies that could affect ion bombardment distribution. Lastly, meteoroid impacts release material into the exosphere. There are different sources of meteoroids in the inner solar system (e.g., Pokorný et al. 2018; Janches et al. 2021). Most of the interplanetary dust is distributed in a disk in the ecliptic plane. In addition to the steady flux of meteoroids, there are occasional crossings with dust streams from comets (e.g. meteoroid showers; i.e.: Killen and Hahn 2015). Understanding the spatial and temporal variability of these external drivers is important to interpret the observation on these spatial and temporal scales, both ground-based and with spacecraft.

3.1 Ions and Electrons

MESSENGER magnetic field and ion measurements provided a huge amount of information about the interaction between the Sun and the hermean magnetosphere. Moreover, the observation and analysis of Flux Transfer Events (FTE) showed that this is the most intense and common way to transfer particles from the solar wind to the magnetosphere (Raines et al. 2015). In the cusps, the solar wind is channelled downward by FTE in form of filaments, FTE showers are frequently observed and are associated to Na^+ - group enhancement probably released after direct ion sputtering of solar wind onto the surface (Fig. 3, Sun et al. 2022).

The iCME impact onto the Mercury's magnetosphere could produce a strong magnetopause compression, in extreme cases the magnetopause is so close to the planet that almost the whole dayside surface is exposed to ion impacts (Slavin et al. 2019). The Na ground-based observations obtained by THEMIS telescope during an iCME encounter with Mercury seems to validate this interpretation showing a variable Na exosphere distributed at mid latitudes in nominal conditions that expands to the whole dayside at iCME passage (Orsini et al. 2018), but much more observations of IMF and local solar wind simultaneously to exosphere imaging at high-time resolution are required for a confirmation of this scenario.

Anyway, the increase in the statistics of Na exosphere measurements at Mercury during different solar activities could not be enough to explain the complex behaviour of the Na exosphere and its relationship with the impacting plasma. For a final proof of the process that generates these observed planetary ion populations and causes the exosphere variability, a full set of simultaneous observations would be needed, from driver to the resulting release. We need measurements of

- the upstream solar wind and IMF for evaluating how the external conditions affect the plasma precipitation,

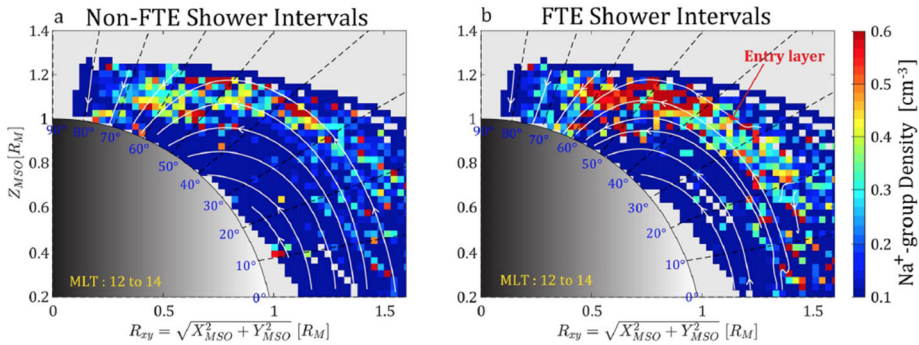


Fig. 3 The magnetic field topology as well as MESSENGER’s spatial distribution measurements of the sodium-group (Na^+ -group) ions during (a) intervals without flux transfer event (FTE) showers and (b) intervals with FTE showers, shown in the R-Z plane. Colors indicate the observed density of the Na^+ -group ions. The white lines represent the magnetic field lines obtained through the average magnetic fields measured by MESSENGER during the intervals without FTE showers and with FTE showers, respectively. (Sun et al. 2022)

- plasma and magnetic field in situ measurements to characterize the plasma directed toward the surface,
- mapping of the area where particles are precipitating, obtainable by the detection of back-scattered and neutralized impacting ions,
- characterization (temporal and spatial variation in densities, mass components and vertical profiles) of the exosphere released after ion precipitation events,
- measurements of planetary ions directed outward from the planet.

While the single-spacecraft mission, MESSENGER, could not observe all these targets simultaneously, this ambitious goal will be addressed at Mercury thanks to the ESA-JAXA BepiColombo mission, which was launched in 2018. In fact, two spacecraft (Mio and Mercury Planetary Orbit – MPO) will be placed in orbit around the planet in 2025. In this way, the external conditions will be monitored together with the close-to-surface populations (Fig. 4, Milillo et al. 2020).

At Mercury the interaction scenario, i.e. the precipitation path, is even more complicated by the induction currents generated by the solar wind plasma flux in the large metallic core close to the surface. In fact, during fast events of magnetic compression, the induction currents act against the compression of the day-side magnetosphere (Jia et al. 2015, 2019; Dong et al. 2019). Eventually, the global current system within the magnetosphere and the surface is still an open question that can be solved only by multi-vantage point observations that allow discrimination between the inner and outer magnetic components.

Transport of plasma and magnetic flux from the dayside to the nightside loads the magnetotail with plasma, until it is released by reconnection in the tail (Slavin et al. 2021; Imber and Slavin 2017). This process accelerates plasma toward the nightside of the planet, where a fraction of it may impact the surface near the open/closed field line boundary in the plasma sheet horns, that are located at mid latitudes in the northern hemisphere and at lower latitudes in the southern hemisphere where the boundary is shifted northward together with the internal magnetic dipole (Raines et al. 2015). Different planetary ions, directly released from the surface or generated in the exosphere after photoionization, circulate into the magnetosphere, part of these populations, after experiencing acceleration processes, can impact the surface thus generating a second generation of exosphere (Milillo et al. 2020). The effect on

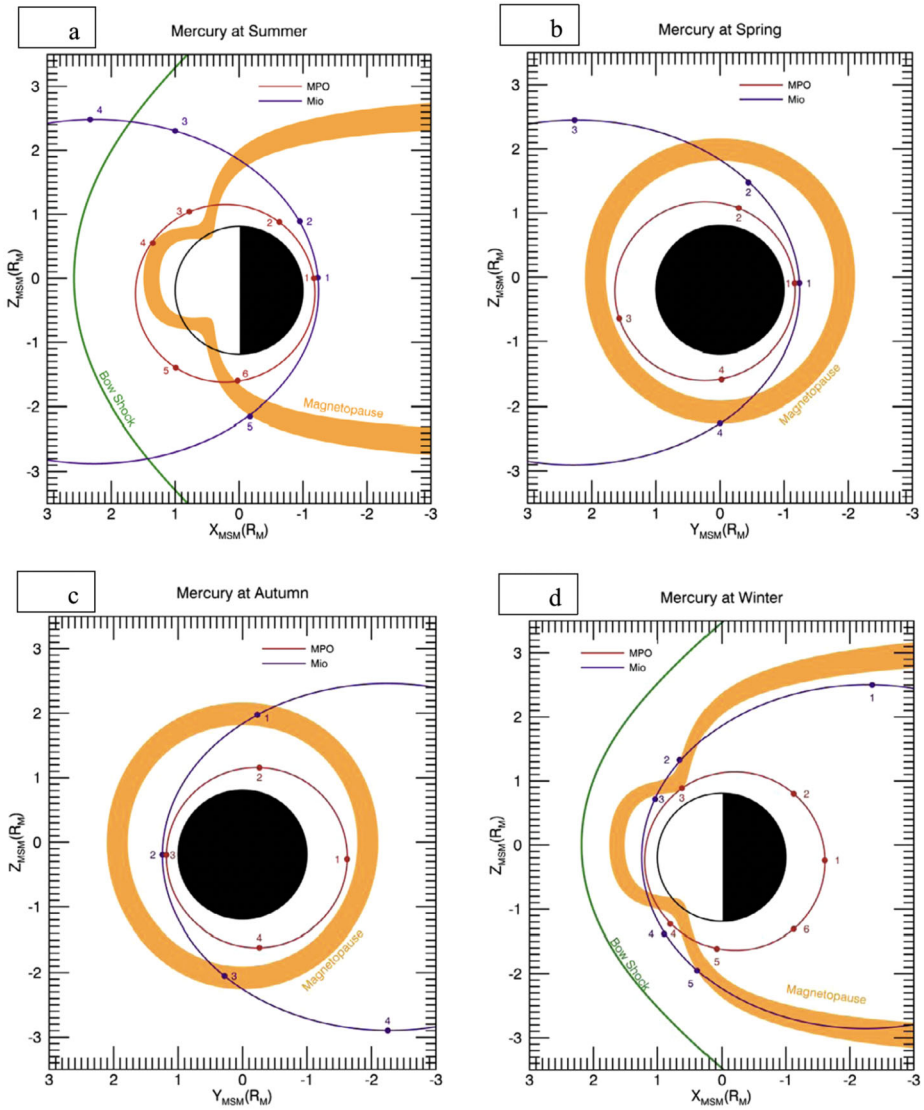


Fig. 4 Schematic view of perihelion/Summer (a), Autumn (c), aphelion/Winter (d) and Spring (b) BepiColombo orbits configurations (from Milillo et al. 2020). The planet Mercury is represented by the black circle (filled in the nightside). The red and blue lines show the MPO and Mio orbits after insertion. The orange area represents the variability (1σ) of the magnetopause according to the 3D-model of Zhong et al. (2015) which includes indentions for the cusp regions. The green line represents the approximate position of the bow shock (Winslow et al. 2013)

the exosphere of the nightside ion precipitation has still not been investigated since nightside exosphere measurements were not allowed with the MESSENGER UV-Vis spectrometer MASCS. The in-situ measurements by BepiColombo/MPO with the SERENA-STROFIO mass spectrometer performed simultaneously with ion measurements will allow the investi-

gation of the nightside exosphere generation processes for the first time (Milillo et al. 2020; Orsini et al. 2021).

Signature of electron impact onto Mercury's nightside surface has been identified by the X-Rays observations of MESSENGER (Lindsay et al. 2016) in agreement with analysis of depolarization signatures by Dewey et al. (2020). The electron impact mapping has been obtained mainly for the northern hemisphere since MESSENGER orbit was highly eccentric with perihelion close to the north pole. The ESD produced after the impact of the electrons onto the surface has never been observed. The simultaneous observations of electrons and volatile components of the exosphere are required to obtain hints on the efficiency of this process. The BepiColombo mission will provide a more accurate electron precipitation mapping at both hemispheres thanks to the optimal orbit of the MPO spacecraft; the observations of the signatures of reconnection and depolarization from Mio spacecraft in the magnetotail, will help to identify the origin or trajectory of the impacting electron population; furthermore, the measurements of the nightside volatile component of the exosphere obtained with a mass spectrometer will allow to evaluate the effect of the electron stimulated desorption where most of other surface release processes are not active (Milillo et al. 2020).

Generally, the interpretation of single- or double-point observations in the magnetosphere requires advanced simulations of ion circulation in Mercury's environment allowing to follow the particle trajectories and to connect the measurements (see Sect. 6).

In contrast to Mercury, ions precipitate more freely onto the lunar surface. The Moon is exposed to plasma environments with different plasma characteristics as it orbits around the Earth. It spends nearly a quarter of its orbit in the terrestrial magnetosphere, when we see it as full Moon, and the rest of the time in Earth's magnetosheath or in the solar wind (Kallio et al. 2019). Outside the terrestrial magnetosphere there are highly variable conditions (from low to fast streams, from low densities solar wind to dense ICME events) (Wurz et al. 2022). When the Moon is in the solar wind, the general distribution of solar wind impact onto the surface is only driven by the geometry (a cosine law from the subsolar point) and it is negligible at the night side. The lunar surface is charged positively on the dayside due to the emission of photoelectrons from the dayside and negatively on the nightside due to the difference between the electron and proton fluxes (Halekas et al. 2011). This makes it possible to have ion precipitation also in the regions close to the terminator by deflected solar wind (Halekas et al. 2011; Vorburger et al. 2016). Sputtering by electrons is also thought to be the dominant erosion process for potential surface frosts in lunar cold traps (Farrell et al. 2019).

The situation is different in the localized regions where there are magnetic anomalies. Here the solar wind is deflected and flows along the mini magnetospheric-cavities, thus impacting the surface at the boundary of the region and leaving the magnetized region shielded (Futaana et al. 2013), the estimated difference being about 50% (Vorburger et al. 2013). This has been demonstrated by the IBEX and Chandrayaan-1 observations of the back-scattered neutralized solar wind (McComas et al. 2009; Wieser et al. 2010; Vorburger et al. 2012, 2013) and of the reflected electrons and ions observed from and Chandrayaan-1 and SELENE (Anderson et al. 1975; Lue et al. 2011; Saito et al. 2010, 2012). The velocity distributions of downward-travelling particles are altered from those of the pristine ambient plasma also after the interaction with plasma waves in the near-Moon space (Halekas et al. 2012; Harada et al. 2014a,b; Fatemi et al. 2015; Wurz et al. 2022). The detailed precipitation map of the solar wind at the magnetic anomaly regions together with local plasma simulations will allow us to thoroughly analyse the interaction in these complex regions. This could aid in the characterization of lunar sites for human colonization.

When the Moon passes through the terrestrial magnetotail both sunward and anti-sunward flows commonly exist (Troshichev et al. 1999; Øieroset et al. 2002). Heavy ions

could be present especially during geomagnetic activities (Seki et al. 1996; Poppe et al. 2016). The intensity of back-scattered particles is higher in these conditions, and it seems less sensitive to the magnetic anomalies, hence the shielding is less efficient. This is probably due to higher plasma temperatures and energies, and low Mach number (Allegrini et al. 2013).

When the Moon is located in the foreshock region, the high-energy ions back-streaming from the bow shock can directly access the lunar surface (Benson et al. 1975; Nishino et al. 2017) and produce ion sputtering. We still do not exactly know which fraction of these ions impact the nightside lunar surface.

The plasma monitoring upstream of the Moon could be obtained in the future by the international space station Deep Space Gateway, that will be located between the Earth and the Moon orbit and that will include a full plasma package (Dandouras et al. 2023). This continuous monitor coupled with exospheric measurements performed by dedicated missions in orbit close to the Moon surface (ISRO Chandrayaan, NASA-ESA Artemis and NASA CLPS, Chinese Lunar Exploration programs, Korea Pathfinder Lunar Orbiter – KPLO) will allow to perform statistical studies on plasma and exosphere variations.

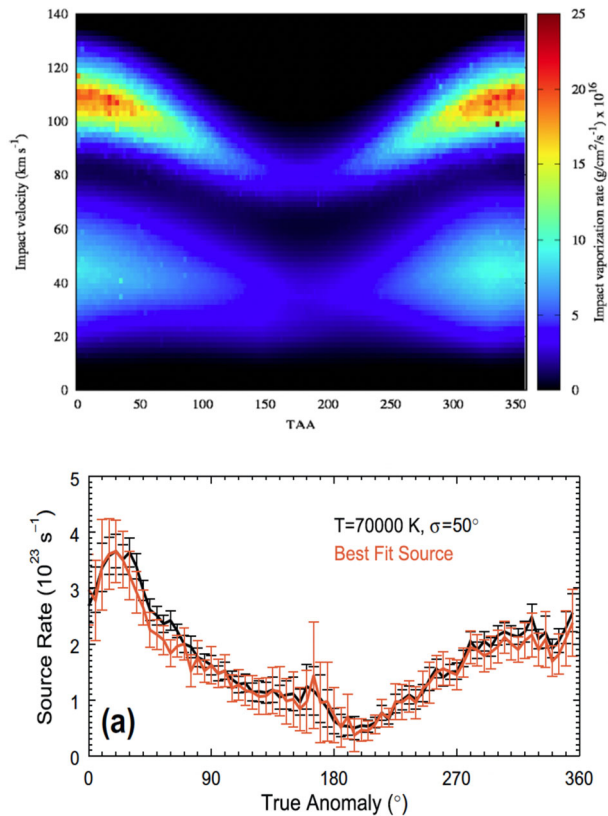
In spite of the extensive modelling of the sputtered component (e.g., Wurz et al. 2007; Sarantos et al. 2012), the detection of the exosphere generated by ion sputtering is difficult because of low energy range and low intensity of the products. Little evidence of an energetic exosphere potentially produced by this sputtering has been obtained (Wang et al. 2021). Vorburget et al. (2013) reported that, when the solar wind was at high-helium content, the Chandrayaan-1/CENA sensor measured a slightly higher heavier/light mass ratio than at nominal solar wind conditions. Most of the measurements were due to backscattered solar wind; nevertheless, this observation could be the signature of higher sputtering efficiency due to He^{++} impacts (supposed to be about 20% more than the yield of H^+). The sputtered density is expected to be much reduced over large magnetic anomalies as the deceleration of solar wind protons reduces the sputtering yield (Poppe et al. 2014); in fact, several lunar magnetic anomalies are also correlated with lunar swirls (e.g., Denevi et al. 2014), this seems to confirm local intense space weathering activity (see also Sect. 2).

3.2 Micrometeoroid

While micrometeoroids refill the surface with gardening, their impacts onto the surface of airless bodies are surely one of the major drivers of surface release, especially for refractories and molecules that are tightly bound to the minerals (Janches et al. 2021). The release material is proportional to the incoming flux and to the velocity of the meteoroids (Cintala 1992). Different origins have been identified for the micrometeoroid populations at Earth's and at Mercury's orbits. The main sources for the inner solar system meteoroid populations are particles originating from Main Belt Asteroids (MBAs), Jupiter Family Comets (JFCs), Halley Type and Oort Cloud Comets (HTCs and OCCs) (Janches et al. 2021). Each family of meteoroid has a characteristic trajectory and velocity distribution, so that anisotropic distribution of meteoroids in arrival direction may produce seasonal, diurnal and planetographic variability of incoming meteoroids (Fentzke and Janches 2008; Janches et al. 2018; Pokorný et al. 2017; Janches et al. 2021).

In particular, measurement of Ca and Mg in the exosphere of Mercury showed that the micrometeoroid impact vaporization is the main source mechanisms for these refractory species, producing a clear asymmetric distribution toward dawn (Mercury's ram direction) and a clear seasonal modulation proportional to the expected dust distribution (Burger et al. 2014; Pokorný et al. 2018) (Fig. 5). In fact, the eccentric and inclined (7° with respect to

Fig. 5 Above: Total vaporization flux as a function of True Anomaly Angle (x-axis), and the impact velocity (y-axis) at Mercury. The units are $\text{g cm}^{-2} \text{ s}^{-1}$ per 2 km s^{-1} bin. From Pokorný et al. (2018). Below: Ca source rate determined using a source with $T = 70,000 \text{ K}$ (black curve) compared to sources derived from MESSENGER/MASCS data (red curve with error bars) along Mercury's year (Burger et al. 2014)

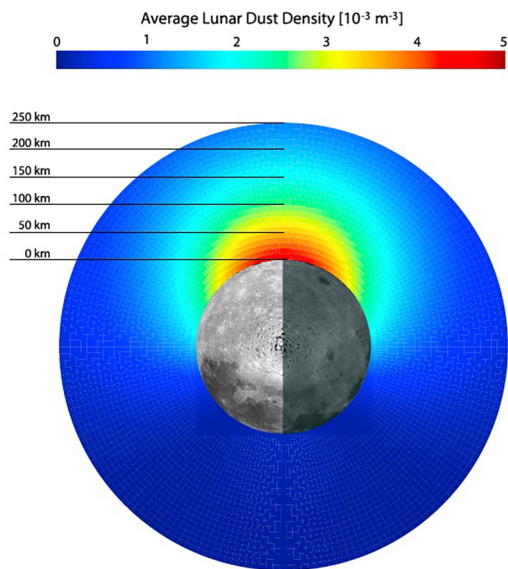


the ecliptic plane orbit where the dust disk is distributed) orbit of Mercury passes through highly variable micrometeoroid intensities. Regions closer to the Sun have higher micrometeoroid densities and the relative velocities with the planet are higher, as well. Kameda et al. (2009) reported a relation of the exospheric Na global intensities with respect to the distance from the expected dust disk, but Milillo et al. (2021) reported that the Na distributions generally peak at the hemisphere farther from the dust disk (North above the disk and South below it). The increase of global Ca content in the exosphere at the comet 2P/Encke dust stream crossing was observed by MESSENGER/MASCS UV spectrometer (Fig. 5 bottom panel) (Killen and Hahn 2015), but the intensity of this increase is still to be quantitatively explained (Killen 2016; Plainaki et al. 2017).

For the first time, BepiColombo mission will be able to measure the dust distribution from the Mio spacecraft and the exospheric distributions of different species and molecules (Milillo et al. 2020).

Regarding the Moon, the LDEX measurements provided compelling evidence that our understanding of how meteoroids influence the lunar surface must be revisited. A detailed description of these findings is presented in Janches et al. (2021). In summary, the measured fluxes showed that the Moon is engulfed in a permanently present, but highly variable dust exosphere that is most dense at 5–8 hrs of lunar local time, with a peak density tilted somewhat sunward of the dawn terminator (Fig. 6). Several authors have shown that Long Period Comets (LPC) produced meteoroids (i.e., HTC and OCC; Janches et al. 2021) should play a major role in the production of the observed ejecta cloud in the Moon's equatorial plane.

Fig. 6 The modelled annually averaged lunar dust density distribution for particles with a $\geq 0.3 \mu\text{m}$. The Sun is on the left and the apex motion of the Moon about the Sun is towards the top of the page (Szalay and Horányi 2016)



Furthermore, the cloud density is modulated by both the Moon's orbital motion about the Earth and about the Sun. The tilting of the ejecta cloud toward the Sun seems to be more pronounced earlier during the LADEE mission (November 2013), while the LDEX signal became more centred around the dawn terminator toward the end of the mission (April 2014) showing a clear seasonal variability.

Efforts of modelling the influence of meteoroids on the lunar surface parallel those at Mercury and differ again on the meteoroid populations included in the different treatments. The effect of gravitational focusing plays a significant role in shaping the lunar and terrestrial meteoroid environment and the night-side to day-side asymmetry, although reproduced by the models, still have unknown physical effects that require further investigation.

The absolute mass flux of meteoroids onto the Moon is also a critical quantity that cannot be fully constrained with LDEX observations. For example, the total flux of MBA meteoroids cannot be constrained by modelling LDEX observations because they produce a negligible contribution to the total ejecta mass production rate due to their very low velocity. Furthermore, to stay consistent with Earth-based estimates of the mass flux ratio of short-to-long period comets (Carrillo-Sánchez et al. 2016), Pokorný et al. (2019) finally concluded that the total mass accreted at the Moon is approximately 1.4 t/day assuming 43.3 t/day at Earth, where the individual contribution of meteoroid populations are: JFCs $\sim 72.6\%$, HTC $\sim 12.8\%$ and OCCs $\sim 10.0\%$. An important note is that these results represent one of many possible fits to the available LDEX measurements and that the solution space to provide a similar or better fit is wide due to the limited selenographic coverage of LADEE.

JFCs meteoroids are concentrated close to the ecliptic plane, arriving from direction towards and away from the Sun (helion and anti-helion sources). HTC and OCC meteoroids impact the Moon mainly towards the apex direction while MBA meteoroids have radiants ranging from all directions and are hence able to populate the anti-apex source. Like at Earth, the apex source has average impact velocities exceeding 55 km/s, while the toroidal and helion/anti-helion sources are in general populated by meteoroids a factor of two slower. Due to the smaller gravitational focusing on the Moon, JFC and MBA meteoroids contribute 2.5 and 5 times less in terms of the mass flux to the lunar meteoroid environment, respectively,

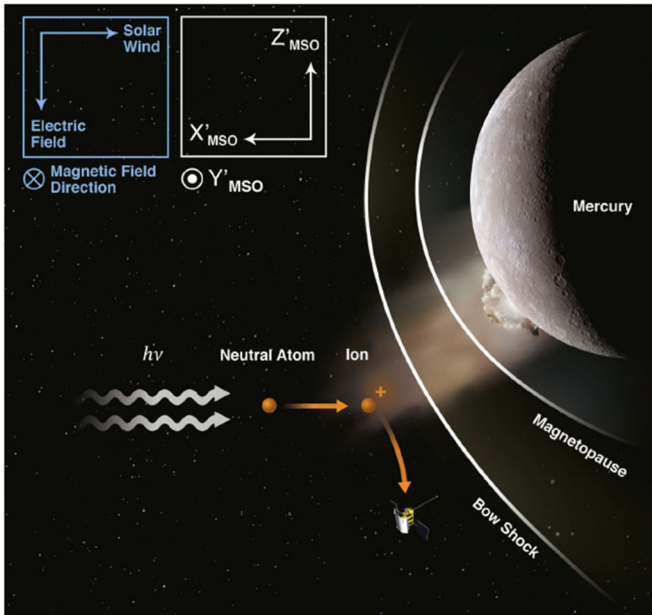


Fig. 7 A schematic from Jasinski et al. (2020) showing the photoionization of neutral particles released from the surface of Mercury due to a large impactor. The newly photoionized particles were observed as pickup ions by the MESSENGER spacecraft in the solar wind upstream of the bow shock

than at Earth. As a result of the broad latitude distribution of cometary impactors, the entire lunar surface can be exposed to impacts with velocities as high as 30 km/s, where the near ecliptic directions can produce impacts with velocities up to 72 km/s.

Finally, Pokorný et al. (2019) showed that the meteoroid mass flux and, consequently, the impact vaporization flux and ejecta mass production rate experience yearly and monthly variations that can be well represented by a sum of two sine functions with periods of one year and 29.5 days (synodic period of the Moon). The mass flux variations amount to 3.3% of the yearly average mass flux, while monthly variations amount to only 0.2%. For the case of the impact vaporization flux accounts for 6–8%, while monthly variations are around 4–5%. When the full spectrum of impact velocities is taken into account, the apex/dawn terminator source is dominating both the impact vaporization flux and the ejecta mass production rate for any day of the year. This expected total vapor rate is higher than considered in lunar exosphere models (Sarantos et al. 2012), meaning that the role of impact vaporization in supplying the lunar exosphere with metals may have been previously underestimated, especially for species like Na and K which do not condense.

In addition to the quasi-continuous flux of micrometeoroid, which contribute to the exosphere generation, sporadic impacts of meteoroid bigger than 1 cm must be considered. Their frequency is much lower than the impact rate of the micrometeoroid populations, but their contribution to the instantaneous exosphere density could be dominant (Mangano et al. 2007). In fact, MESSENGER revealed the signature of a major meteoroid impact by detecting the pickup planetary ions in the solar wind upstream of the bow shock probably originating from atoms released after a meteoroid impact and subsequently photoionized (Jasinski et al. 2020) (Fig. 7).

We can expect to record much more detections of these events during the BepiColombo mission lifetime including mission extensions (Mangano et al. 2007). It will be possible to search for the impact crater after these events, thanks to the possibility to obtain high spatial resolution imaging of the surface with the camera suite SimbioSys on board of MPO (Cremonese et al. 2020).

In the incoming decade, dust detectors on board DESTINY (Krüger et al. 2019) and IMAP (McComas et al. 2018) missions will allow monitoring of dust at 1 AU, thus providing an important tool for constraining the meteoroid contribution to the lunar exosphere formation.

3.3 Solar UV Variability

Together with ions, electrons, and micrometeoroids, solar photons in the UV range arriving at the surface are an important factor in the release of some species softly bound to the surface, such as volatiles and alkali atoms. In fact, the PSD process releases atoms or molecules adsorbed on the surface, i.e., species that are not chemically bonded within a mineral (Wurz et al. 2022).

At Mercury and the Moon, the PSD is considered the most efficient surface release process for Na when coupled with the action of ion impact (Mura et al. 2009). In fact, the vertical profile of the Na densities at Mercury is consistent with a characteristic temperature of 1200 K, compatible with the PSD energy distribution (Cassidy et al. 2015).

The solar photon fluxes exhibit short time variability due to the emission of solar flares and long-time variability due to the orbital eccentricity especially on Mercury. The intense photon flux varies by more than a factor 2 along the orbit of Mercury, due to the inverse square distance dependence). At the Moon the UV flux is less variable along the orbit that is less eccentric.

Variabilities of some orders of magnitudes in EUV emission are expected in less than few hours during solar flares (Werner et al. 2022); in the Ly α line an increase about 20% has been observed in major flares (Milligan 2015).

Finally, along the 11-year solar cycle the Ly α flux varies in the range $(3.5\text{--}6) \cdot 10^{11}$ ph/(cm² s) at 1 AU and at solar maximum the flare index (describing the number, size and brightness of the flaring areas (Ozguç et al. 2021)) reaches a value up to 20 times the solar minimum periods (Bruevich and Yakunina 2017).

It is estimated that in the early phases of the Sun 10- or 100-times higher UV fluxes were emitted (Ribas et al. 2005), so that we can expect that PSD was even more relevant in the first stages of the Mercury's history (Orsini et al. 2014).

To better constrain the effect of UV variability in the volatile components of the exospheres we would need simultaneous short- and long-term observations of the Sun.

For Mercury, the BepiColombo mission will provide systematic observations during its nominal lifetime (2 years) and possible extensions (one or two more years) (Benkhoff et al. 2021).

4 Open Points on Exosphere Investigations

Being collisionless, a surface-bounded exosphere can be considered as the sum of different single-species exospheres. In fact, past exospheric observations of airless bodies revealed quite different distributions and dynamics of the different species around the body, mostly depending on chemical properties. The main families can be grouped in: highly volatiles

and water groups, refractories and molecules and moderately volatiles alkali (Grava et al. 2021a; Schörghofer et al. 2021; Leblanc et al. 2022).

The volatiles are those elements are weakly bound to the surface; they are easily released and have a low sticking efficiency. Examples of this group are hydrogen, water groups, helium and methane. The refractories are elements with a very high melting point and strongly bound to other atoms, and above all they are easily oxidizable. They are on the opposite scale of surface-exosphere interaction compared to volatiles. The alkali metals, like Na and K, have their outermost electron in an s-orbital and this shared electron configuration results in a high reactivity.

4.1 Volatiles and Water Group Species

In general, exosphere densities of solar-wind-derived volatiles are expected to scale with the solar wind flux: the higher the flux of solar wind ions of a given species, the higher the exospheric content of the corresponding neutral species. This is the case for example with helium: on the Moon, the lunar exospheric helium density decreases when the Moon enters in Earth's magnetotail (Feldman et al. 2012), and the lunar surface is shielded from the solar wind bombardment (in this case from alpha particles). When the Moon exits the magnetotail a few days later, the exospheric density of ^4He quickly recovers to nominal levels (Grava et al. 2021b). Observations from LADEE showed also that exospheric He responds to specific solar wind streams (Benna et al. 2015). But for other solar-wind derived species, this relationship is not as straightforward. Neon, for example, is also a solar-wind-derived species, but its photo-ionization lifetime is 3 months. Therefore, it does not show short-term variations due to solar wind fluctuations. It does show long-term fluctuations: the pre-dawn exospheric density measured by LACE during nominal solar wind conditions was about one order of magnitude lower than the exospheric density measured by LADEE from orbit, during a iCME. However, modelling efforts by Killen et al. (2019) revealed that the surface-exosphere interaction of neon is not as simple as previously thought: the neon lifetime required to match LACE data is 4.5 days, 20 times shorter than the photo-ionization lifetime for nominal solar wind conditions (100 days), and comparable to helium, a gas that is lost mainly through thermal escape.

At Mercury, close to subsolar point Mariner-10 detected a H double temperature vertical density profile that is justified for highly volatile species that mix population thermalized with the dayside surface (420 K) together with low temperatures population thermalized with the night side (110 K) and circulating in the dayside (Hunten et al. 1988; Grava et al. 2021a). Exospheric hydrogen was detected also at the Moon in molecular form H_2 (Stern et al. 2013). The implantation of solar-wind protons into the lunar soil generates an OH-veneer and, in small amounts, molecular water, a subject reviewed in Schörghofer et al. (2021) (Fig. 8). These interactions of the solar wind with the amorphized grain surface layers need to be understood in far more detail, so we can quantify the production rate of H_2 versus H_2O and the degree of latitudinal and possibly diurnal variation of the OH surface population. Another central question is to what degree water molecules can repeatedly hop on the lunar surface, which defines the ability of an exosphere to transport water to polar cold traps.

The Moon offers an ideal laboratory to study the fate of solar wind ions recycled as neutral to form the exosphere of an airless body. One example is the neutralization of solar wind alpha particles to create helium. The recent finding that observations of lunar helium are consistent with full thermal accommodation with the surface (Grava et al. 2021b) suggests that, even if it is expected that a good portion is back-scattered and should not interact with grains

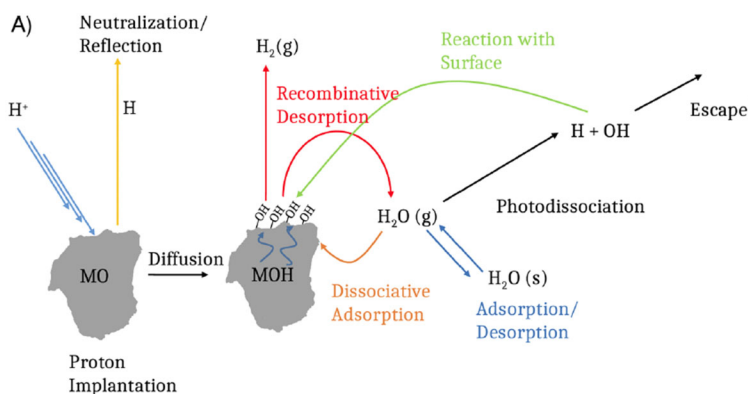


Fig. 8 Kinetic scheme for the solar-wind-induced water cycle on the surface of Mercury. Upon heating, a reaction takes place between neighboring OH sites (encircled with green) resulting in the formation of gas phase water and an oxygen bridge between cations (Schörghofer et al. 2021)

more than once, some incident helium atoms are expected to experience multiple collisions with different grains of the regolith prior to reflection from the lunar surface, thus losing energy. Methane (CH_4) is another example. It has been detected by LADEE/NMS. Hodges (2016) showed that the recombination of solar wind carbon ions with hydrogen atoms in the soil is a pathway for production of methane in the lunar exosphere (methane can offer insights on the fate of H as well, as pointed out by Tucker et al. 2019). However, carbon-bearing species can also come from micrometeoroids so the conclusion obtained should be taken with some caveats. Hodges (2016) predicted that CO should also be present in significant amounts in the lunar exosphere, owing to its photoionization lifetime, which is 9 times longer than methane's. Unfortunately, artifacts in the mass channel 28 prevented the LADEE NMS from detecting CO, but LACE detected a post-sunrise peak in exospheric density at the same mass channel, which were attributed to either N_2 or CO (Hoffman et al. 1973). Despite the absence of artifacts, LADEE NMS did not detect CO_2 . More measurements are clearly desired to understand the solar wind ions recycling at the lunar surface.

A central role of the exospheres of condensable species is their ability to transport molecules from any location on the surface to cold traps, where they accumulate in condensed form as ices. At the current state of knowledge, these processes are expected and plausible, but they have never been proved. The definite detection of an exosphere of molecular water on a large airless body with a silicate-rich surface would be a crucial observation. The few existing observations are limited by ambiguities. CHACE-1 made a one-time measurement on the Moon (Sridharan et al. 2010) that exceeds the upper limit from the Apollo era (Stern 1999). LADEE did not distinguish between OH and H_2O (Benna et al. 2019). On Mercury, no instrument has yet allowed such a measurement to be performed. And also on Ceres, for example, most attempts failed to detect an H_2O exosphere, with two exceptions involving instrumentation that is no longer available (Schörghofer et al. 2021). In total, no measurement reveals whether such an exosphere is global or localized in the shape of a plume. Definitive observations of a water exosphere and its properties would greatly advance our framework of understanding exospheres and ices on these planetary bodies.

Another key task is to determine the ability of exospheres of condensable species for lateral transport. In other words, whether molecules undergo repeated ballistic hops or are chemisorbed indefinitely on the surface after the first hop. So far, observations have provided only indirect evidence for or against this hypothesis, and, likewise, theory has been used to

argue for or against repeated ballistic hops. The answer to this question may to a large degree determine the abundance of water on the Moon, an essential resource for sustained robotic and human presence on the Moon.

The interaction of H and H₂O with radiation-damaged silicate-rich grains needs to be understood far more comprehensively. One aspect, already mentioned, is the ability of H₂O molecules to repeatedly desorb. The other is the rate at which solar wind interactions generate molecular water by interaction of solar wind protons with metal oxides. The activation energies and processes on these complex amorphized surfaces can be investigated with further laboratory measurements and solid state modelling.

Volatiles are also useful to study outgassing from the interior. Evidence from outgassing from the interior of the Moon has been provided by several instruments. The Apollo 17 LACE mass spectrometer deployed on the lunar surface detected ⁴⁰Ar, which is the radiogenic product of the decay of ⁴⁰K within the crust. A small fraction of the lunar exospheric helium, also detected by LACE, is also endogenic, coming from the radioactive decay of thorium and uranium (Hodges 1977). The Alpha Particle Spectrometers (APS) onboard the Apollo 15 and 16 command modules and Lunar Prospector detected alpha particles produced by the decay of radon and polonium (Gorenstein and Bjorkholm 1973; Bjorkholm et al. 1973; Lawson et al. 2005). Data collected from these two types of instruments reveal that the outgassing of these radiogenic elements is variable, both spatially and temporally. Some of the regions that were actively outgassing radon during the Apollo era were not active during the Lunar Prospector survey, 30 years later. Radiogenic gases concentration on the Moon appears to peak in pyroclastic deposits and prominent young craters such as Aristarchus and Alphonsus, and at the mare-highlands boundaries. These are all regions with either a thin crust (such as in pyroclastic deposits) or a fractured terrain (the Maria edges, such as the landing site of Apollo 17), which both facilitate the outgassing from the lunar interior into the exosphere (Fig. 9). Some radiogenic gases detected so far (radon, polonium) condense on the cold lunar nightside surface and on PSRs. Therefore, long-term monitoring of the exospheric density of these gases can constrain the outgassing rate and thus the amount of incompatible elements thorium and uranium, benefiting the study of the origin of the Moon (and Mercury, assuming these elements will be detected by BepiColombo).

4.2 Refractories

Being very “sticky”, i.e., with a very high activation energy for desorption, refractories are released only by energetic processes, such as MIV and sputtering by energetic ions, mostly from the solar wind. As such, they are important species to study the response of surface-bounded exospheres to changes in the external environment (solar wind and micrometeoroid flux).

For certain species a double mechanism has been proposed. For example, for calcium, detected at Mercury, it has been suggested that first it is released from the surface by an energetic process (MIV or ion sputtering) in the form of calcium oxide (CaOH, Ca(OH)₂, or CaO). After the first plume expansion, it is subsequently dissociated by photons or electrons, or via unimolecular decay, with an excess of energy, resulting in different molecules or atoms with additional energy imparted to Ca products (Berezhnoy 2018). The final products after the impact depend on the quenching temperature of the expanding cloud that is expected to be in the range 3000–4000 K. At temperatures ≤ 3750 K in the impact-produced cloud Ca(OH)₂ dominates over both atomic Ca, CaO and CaOH, while at higher temperatures it is considered that the predominant form of the initial calcium ejecta is CaO (Berezhnoy 2018). Recently, Moroni et al. (2023) showed that observed Ca density at Mercury can be quantitatively explained only if the quenching temperature is below 3750 K.

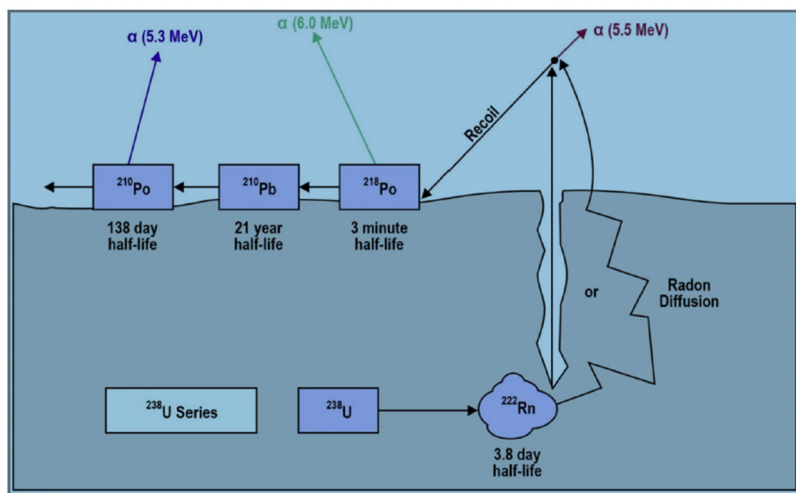


Fig. 9 Scheme of radon decay, with alpha particle energies pertaining to each product. The short half-life of radon makes it a useful species to constrain regions of active outgassing (Grava et al. 2021a or Grava et al. 2021b, adapted from Lawson et al. 2005, JGR, 110)

The release near dawn, necessary to explain an excess of Ca detected there (Burger et al. 2014), is consistent with micrometeoroid bombardment, which peaks at dawn due to the motion of the planet. Moreover, a regular excess concentration of Ca in the Hermean exosphere at certain true anomaly angles has been explained by the intersection of Mercury's orbit with that of comet 2P/Encke (Killen and Hahn 2015). Nevertheless, as mentioned in Sect. 3.2, a quantitative estimate of the excess Ca produced has not yet been obtained (Killen 2016; Plainaki et al. 2017). Other features in the yearly Ca distributions, like a decrease while approaching the perihelion or a secondary maximum while approaching the aphelion, still need to be explained, as well (Fig. 5 bottom panel).

This suggests that other mechanisms are likely at play, waiting to be uncovered by future observations from the ground or from BepiColombo's suite of instruments. It is also possible that Ca is released in another molecular form, such as CaS. Mg is another species of interest. Detected at Mercury by MESSENGER, as for Ca, the temperature (energy) of Mg atoms in the exosphere is twice that expected from MIV. Mg is important because of the link to Mg-rich regions at the surface. Merkel et al. (2018) showed that the exospheric Mg abundance peaks when Mg-rich regions are exposed at dawn at perihelion.

More observations, laboratory measurements, and simulations are needed to study the exospheric distribution and dynamics. In particular, much more atomic and molecular species are expected to be released into Mercury's and Moon's exospheres. The nightside exospheres are still almost not constrained by measurements since most of the observations, especially for Mercury, have been performed by remote sensing instruments that collect emission lines of photon-excited atoms.

4.3 Alkali Metals

Alkali more than other species, like refractories and highly volatile components are released by complex mechanisms. Due to their high reactivity but relatively low binding energy with the surface makes their release is affected by thermal radiation, UV photons, ion and electron

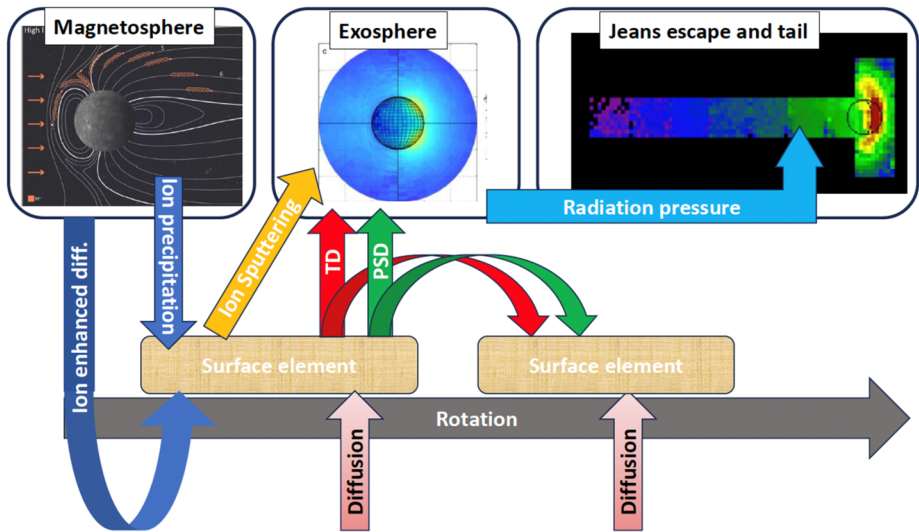


Fig. 10 Scheme of Sodium circulation between Mercury’ surface and exosphere. It can be applied to the lunar Na exosphere by considering a different plasma precipitation map (revised from Leblanc et al. 2022)

impact and micrometeoroid impact, radiative diffusion inside the regolith, and triggered by energetic particle radiation and chemical modification of the surface (Wurz et al. 2022; Leblanc et al. 2022). On the other hand, they (especially Na) are the species most observed in the environment of Mercury and the Moon since Na and K have two resonance emission lines in the visible range, close and near the solar emission maximum, so they are easily observable by ground telescopes.

Beside the set of observations and modelling that could help to progress in our understanding of the Na and K exospheres around the Moon and Mercury, the relations between magnetosphere, surface and exosphere can be specifically addressed by combining various observations and new theoretical and experimental developments.

The very first external driver that controls the alkali exospheres of the Moon and Mercury is the solar photon flux. This flux has three different effects on the sodium and potassium exospheres. First, it contributes to the ejection of these volatiles from the surface by either thermal desorption or by photon stimulated desorption. A detailed description of these two mechanisms can be found in Wurz et al. (2022), as well as in Leblanc et al. (2022) (Fig. 10). The EUV/UV range of the solar photon flux also leads to the photo-ionization of these atoms, which is very probably the most efficient process for creating sodium and potassium exospheric ions. But, the solar photon absorption and emission also induces an anti-sunward force, the solar radiation pressure, at the origin of the very extended exospheric tail at Mercury (Schmidt 2013) but also at the Moon (Baumgardner et al. 2021).

To observe how efficient might be the solar flux might be in controlling the exosphere of Mercury and the Moon, one approach is to image the diurnal and annual variabilities of the exosphere. It needs, however, a large set of observations and the help of models taking into account all possible mechanisms at the origin of the alkali atoms in the exospheres (see Leblanc et al. 2022). For example, waiting for the BepiColombo nominal mission, when we will have in situ detection and global imaging of the Na distributions (Milillo et al. 2020), we need more ground-based observations to obtain a more complete dataset for the investigation of the dawn-dusk Mercury’s seasonal variability (Milillo et al. 2021). In fact,

ground-based observations with dawn/dusk view at all True Anomaly Angle (TAA, i.e., Mercury's angular distance from perihelion) are still not available. Furthermore, we need more statistics for investigating the northern/southern peak occurrence along the orbit.

The two opposite effects in terms of exosphere production and loss, photo-ionization and photon-desorption, are controlled by the same EUV/UV spectral range also during variable photon flux in the solar events. Solar flares are relatively short (few tens of minutes) with respect to the typical time scale of the global exosphere (few hours) which makes any signature in the exosphere difficult to image directly in its neutral component.

Another key driver of the alkali exospheres, that has been highly debated along decades, is the relation between Mercury's magnetosphere and exosphere. It is known since the very first ground-based observations of Mercury's sodium exosphere (Potter and Morgan 1990), that sporadic peaks in sodium emissions at high latitudes exist in Mercury's exosphere. It has been postulated that what controls these maxima was the effect of the precipitating solar wind particles onto the surface which sputtered volatiles in Mercury's exosphere. No evidence for a similar process has ever been observed around the Moon. Actually, the relatively long time scale of this structure (Leblanc et al. 2008) rather suggests that the sodium atoms were not ejected directly from the surface but rather brought to the upper surface by radiative induced diffusion inside the regolith as suggested at the Moon when passing through the Earth magnetospheric tail (Wilson et al. 2006; Sarantos et al. 2008) and for Mercury sodium exosphere (Mura et al. 2009).

But without a simultaneous knowledge of the solar wind conditions, it is extremely difficult to infer the real efficiency of solar wind particles in populating the exosphere. Ground-based observations during iCME (Orsini et al. 2018) were used to infer such a relation. However, this remains very speculative because ground-based observations are also strongly dependent on the Earth atmospheric condition. On the other hand, recent studies (Sun et al. 2022) show that during event of ion precipitation enhancements (Flux Transfer Events) the Na-group ions population above the cusp of Mercury's magnetosphere (interpreted as ionized component of the sputtered material) increases, as well. It implies that any interpretation of the apparent positions and structures of the reconstructed exosphere needs to be done considering the intrinsic limited spatial and temporal resolutions. This is particularly true when the images of Mercury's exospheric emission are obtained on hour time scale (Mangano et al. 2009), a time scale significantly longer than the typical solar wind perturbation duration. Fortunately, ground based observatories able to target Mercury are gradually incorporating adaptive optics which should significantly improve their spatial resolution and allows a much better tracking of Mercury spatial variability induced on short time scales. Moreover, BepiColombo forthcoming insertion around Mercury will provide a new opportunity (after MESSENGER) to correlate in situ solar wind observation with ground based and in situ observations of Mercury's exosphere (Milillo et al. 2020). In the Moon case, high spatial and temporal resolution measurements of Na could allow the investigation of the surface response to solar wind variability especially in proximity of the magnetic anomalies (see Sect. 3).

Some directions of investigations of the alkali exospheres can be summarized as follows (Leblanc et al. 2022):

- In-situ measurements are essential to obtain simultaneous observations of drivers and the resulting exosphere. Thus, detailed study of the effect of impact of iCME or meteoroid showers can be performed by in-situ measurements.
- Ground based observations have the capability to monitor and globally image the Na and K exospheres.
- Modelling developments remain essential to further understand ground based, MESSENGER, and future observations. In particular, these new models should provide a better

description of the interaction between exosphere and surface by introducing a detailed description of the regolith and of the fate of the exosphere through it. The effect of space weathering on the surface release should be parametrized in the models.

- Laboratory experiments have a key role in addressing the weathering of the surface and the effects on the release efficiency.

4.4 Open Points on Exosphere Dynamics, Sources, and Loss

The exosphere composition of the airless bodies is related to the surface composition, weighted by the surface-release process efficiencies and particle dynamics. Information on exosphere composition can be obtained indirectly via heavy ion detection. Planetary ions are mostly generated via photoionization of the exospheric components. The circulation of charged particles in the magnetosphere (in the case of Mercury) or as pick up ions in the solar wind (at the Moon) allows the detection of planetary species at higher distances.

For the Moon the exosphere generation processes are similar to the Mercury case but with different weight and geometry and at lower gravity. Over extended time scales, the different gravity field of Mercury compared to the Moon is expected to have produced differences in exospheric loss according to the efficiency of different surface release processes for different species (Wurz et al. 2010). This would result in an alteration of the surface composition at Mercury, in contrast to the Moon, where the exospheric loss is similar for all refractory elements (Wurz et al. 2007). For example, the Na/K ratio in Mercury's exosphere cannot be simply associated with the primary abundances but different transport and loss must be considered. Both Na and K could be accelerated anti-sunward by radiation pressure, photoionized and captured by the solar wind. However, they can also re-impact the surface and ionized (followed by neutralization) or neutral state. The higher mass of K relative to Na results in a smaller scale height and a larger gyroradius, which may result in more rapid net loss of K (Potter et al. 2002a,b). Taking into account different loss processes, the observed Na/K exospheric ratio may be consistent with an initial abundance close to solar or meteoritic ones (Leblanc and Doressoundiram 2011). On the other hand, in the case of asteroids, gravity is negligible so the exosphere radiates from the body at a net loss, thus a survey of the exosphere gives direct information of the pristine material of the body (Plainaki et al. 2009).

Unfortunately, up to now only measurements at low mass resolution are available in Mercury's environment from MESSENGER. The ion spectrometers on board both Mercury's orbiters of BepiColombo will allow the identification of new species, also the heaviest ones which can be energized and circulated in the magnetosphere (Milillo et al. 2020).

For the Moon, multiple missions with instruments relevant to exospheres and exosphere-surface interactions are expected to launch soon. Already at the Moon are CHACE-2 (a neutral mass spectrometer) (Das et al. 2020) and IIRS the infrared spectrometer on Chandrayaan-2 (already in orbit) (Chowdhury et al. 2020).

MESSENGER UVVS/MASCS observations have clearly shown that the surface composition might have a direct impact on the exosphere composition in the case of its Mg component (Merkel et al. 2018). No similar evidence has been obtained in the case of the Alkali exospheres, even if the high latitude peak in surface density has been tentatively explained by the preferential exospheric sodium reabsorption of the surface in these cold regions (Peplowski et al. 2014). Here again, BepiColombo forthcoming detailed observation of the surface composition combined with in situ and remote observations of the exosphere might help us to improve our understanding of this relation (Hiesinger et al. 2020).

A prevalence of Na emission in the equatorial dawn hemisphere has been first spotted by ground-based observations (Sprague et al. 1997; Potter et al. 2002a,b; Schleicher et al. 2004)

and then confirmed by the MESSENGER/MASCS and by other statistical studies of ground-based images (Fig. 11 panel b) (Milillo et al. 2021). This local time asymmetry has been explained considering a global Na circulation in the exosphere and preferred condensation of the alkali atoms in the cold regions of the nightside surface (Mura et al. 2009). The MESSENGER observations showed a dawn enhancement in the outbound leg of Mercury's orbit but also a prevalence in the equatorial dusk regions between TAA 180° and 270° where the surface exposed at lower average temperatures is sunlit (Cassidy et al. 2016) (Fig. 11 panel a). Such intriguing correlation has been interpreted by the long-term effects of the thermal forcing on the surface capability to trap sodium atoms and to release it when these longitudes face the Sun. How the thermal forcing acts on the sodium surface reservoir is not well understood but could be due to the migration of this volatile species through the first hundred μm of the regolith (Sarantos and Tsavachidis 2020), a migration which would be controlled by the thermal gradient with depth and the radiative induced diffusion of the sodium atoms through the grains and regolith. This peak is not consistent with models of thermal desorption (Leblanc and Johnson 2003; Mura et al. 2009), which have all the Na reservoir, which was built up during night, quickly desorbed – and thus depleted – in the early morning hours. The simulation cannot explain this behaviour without considering extra internal sources of Na (Leblanc et al. 2022).

Porosity also affects mobility on the surface of volatile elements. For alkali atoms (Na and K), similarly to what described in Killen et al. 2004, surface diffusion reduces the net desorption of adsorbates (Sarantos and Tsavachidis 2020). This reduction in desorption rate is temperature-dependent, as it depends on porosity (and thus mobility), PSD yield, and sticking coefficient. Therefore, only when temperature reaches 500 K does thermal desorption start contributing to mobility. On the Moon, the difference in surface grains mobility (diffusion) between K and Na may explain the difference in longevity of Na and K measured from LADEE: K is heavier, so it has reduced mobility, and hence it is more easily photo-destroyed, while Na is more long-lived.

The seasonal variation of the total content of Na in the exosphere shows a distribution with a maximum at aphelion and a secondary maximum at perihelion (Cassidy et al. 2015; Milillo et al. 2021). The drivers able to release Na are maximal at perihelion, so that the observed trend is not straightforward. The suggested explanation of this trend includes the variable contribution of the radiation pressure that pushes Na atoms into the tail and the variable photoionization rate along Mercury's eccentric orbit and thermal inertia of the surface (Rognini et al. 2022). The quantitative justification of an exospheric maximum at aphelion could be due to the combined effect of the 3:2 orbital resonance, and the plasma or micrometeoroid precipitation in the nightside along the orbit (Mura et al. 2023).

Added to the equatorial dawn/dusk asymmetry of the Na distributions, a northward or southward peak prevalence along the TAA has also been discovered by analysing THEMIS ground-based images (Milillo et al. 2021). Specifically, it seems that between TAA 0° and 180° in the outbound leg of the orbit (from perihelion to aphelion) coinciding with Mercury's orbit above the dust disk, the Na peak is observed more frequently at Northern latitudes, on the contrary, the peak is observed more frequently Southward in the inbound leg (TAA from 180° to 360°) coinciding with Mercury below the dusk disk (Fig. 11 panel c). This was not expected; in fact, if the Na surface release was related to ion impact, a predominance of the southward peak, where the cusp and loss cone are expected to be wider because of the magnetic dipole northward shift, should be seen. Furthermore, if the Na surface release was related to ion impact onto the surface, we would not expect a north-south asymmetry linked to TAA. The ion precipitation which in turn is linked to the IMF conditions varies on short time scales and should not depend on season. A link of the north-south asymmetry to TAA

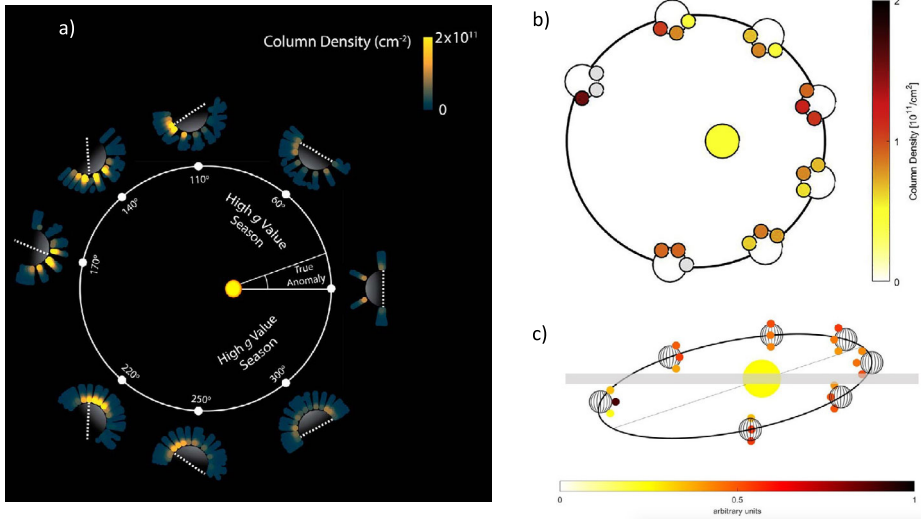


Fig. 11 Averaged Na column density measurements along Mercury orbit. a) equatorial distributions showing dawn/dusk asymmetries derived from MESSENGER/MASCS observations (Cassidy et al. 2016): dawn prevalence between TAA 90° and 180°, and dusk prevalence between 180° and 270°. b) equatorial distributions from THEMIS ground-based observations (Milillo et al. 2021) that confirms the dawn prevalence, but cannot confirm the dusk prevalence observed by MESSENGER. Grey bullets represent no data are available. c) Latitudinal distribution showing that statistically the Northern/Southern peaks are more frequent in the outbound/inbound leg when Mercury is above/below the expected interplanetary dusk disk (Milillo et al. 2021)

opens new hypotheses on the Na generation mechanisms. On the other side it also seems to contradict the role of micrometeoroids impacts that should be higher closer to the dust disk, so in the opposite hemispheres.

Eventually, the importance of the meteoroid bombardment in supplying part of the observed exospheric species has been demonstrated by MESSENGER (as an example in the case of the exospheric Ca and Mg, see Janches et al. 2021 and Grava et al. 2021a). The role of this release process on the alkali population in the exosphere is still not clear. While different studies suggest that it is generally small (e.g.: Wurz and Lammer 2003; Wurz et al. 2010) Kameda et al. (2009) found a correlation between the total Na exospheric intensity and the distance from the interplanetary dust disk, and Gamborino et al. (2019) suggest that the MMIV process is the predominant mechanism populating equatorial high altitudes during the MESSENGER observations. BepiColombo offers a unique perspective thanks to the possibility to quantify the dust flux, its temporal and spatial distributions by Mercury Dust Monitor (Kobayashi et al. 2020). The combination of measurements of the incident dust flux and in situ/remote sensing observations of the various components of the exosphere will be a unique opportunity to fully address investigation the exospheric signatures of the permanent bombardment of the surface by this dust. In fact, this is a key mechanism in the space weathering of the surface but also a major driver of Mercury and the Moon exospheres.

5 Requirements for Advanced Exosphere Modelling

Different MonteCarlo (MC) models have been proposed for describing the exospheres of Moon, Mercury, and asteroids. Although the numerical implementation of how to track millions of test particle trajectories to estimate macroscopically measurable parameters is straightforward, advances are required when it comes to several input parameters that are required or assumed in these models. These include the speed distributions of ejected atoms and molecules, the initial directions of emission, the specification of what occurs during surface-atom interactions (e.g., degree of energy and momentum accommodation), the differing amounts of a constituent at different geographic locations, the directionality of drivers such as incident ions and meteoroids, and other factors (e.g., porosity). Many of these improvements necessitate that new laboratory experiments be performed.

5.1 Modelling Status

Foundational work in the use of Monte Carlo sampling of particle trajectories to estimate exospheric measurables was described by Hodges (1980). Early work focused on explaining measurements of helium and hydrogen-bearing gases at the Moon (Hodges 1973b; Crider and Vondrak 2000), with those papers explaining the algorithms used for the sampling of initial locations and velocities for the few test particles that stand for a much larger ensemble of gas atoms and molecules. The same methods were later applied to simulate argon (e.g., Grava et al. 2015; Hodges 2018), methane (Hodges 1975, 2016), and the water group gas constituents of the Moon (e.g., Crider and Vondrak 2000, 2003; Smolka et al. 2023). The more recent studies include an increasingly sophisticated treatment of the gas-regolith interactions, including the chemical conversions of species on the regolith surface.

Sodium has received much attention in modelling due to the availability of interesting lunar and Hermean observations since the mid 1980s. A first model describing the Na and K exosphere along Mercury's orbit was developed by Smyth (1986) and updated by Smyth and Marconi (1995). This model included a Na population released at 2.6 km/s plus an ambient (thermally accommodated) population generated after the first bouncing onto the surface. It considered the photoionization and the important role of radiation pressure for the escape along the orbit showing the anticorrelation between radiation pressure and Na exosphere observations. This model considered that the escape is replaced by a general source of Na due to micrometeoroid gardening.

The longevity of the exospheric reservoir was since studied with more sophisticated time-dependent sodium adsorbate models. Mura et al. (2009) (IAPS exosphere MC model), Leblanc and Johnson (2003), and Leblanc and Johnson (2010) developed Na exosphere models where the non-uniform planet rotation and the sticking efficiency are taken into account, so that the seasonality of Na release is better described. Additionally, Mura et al. (2009) included the effect of the enhanced efficiency for Na release by PSD after ion impact on the dayside as well as in the night side. By only considering the PSD as the main surface release process for Na and a simple surface thermal model, the observed yearly distribution maximum at aphelion cannot be reproduced. Only by adding a more realistic thermal model, which accounts for the regolith's thermal inertia, can a secondary peak at aphelion be reproduced (Rognini et al. 2022), but still far different than the observed seasonally varying densities (Cassidy et al. 2015; Milillo et al. 2021). Recently Mura et al. (2023) presented an analytical model that explains the peaks at aphelion and perihelion with the combined effect of the 3:2 orbital resonance, and the modulation of the magnitude of sources and losses along the orbit. The processes due to plasma and micrometeoroid impacts produce an

accumulation of un-bound Na atoms in the nightside. These atoms are released when they are exposed to Sun light at dawn following the specific 3:2 spin to orbit resonance. Finally, the enhancement of Na column density at aphelion, and the dawn-dusk asymmetry in the outbound leg are due to the orbit resonance and are stable features of Mercury's exosphere.

As mentioned in Sect. 4, other observables that cannot be reproduced by the state-of-the-art models are a dusk prevalence in Na equatorial exosphere at TAA 180°-270° (Cassidy et al. 2016); the Na increase northward/southward in the outbound/inbound orbit leg, corresponding also to above/below ecliptic plane (Milillo et al. 2021); and the short-term variation of Na and its relationship with the plasma precipitation. Thus, no model yet succeeds in describing the seasonal sodium circulation. One area that merits further study is the incorporation into the boundary conditions of global models of the effects that regolith imposes on gas release because of micro-shadows and Knudsen diffusion (Sarantos and Tsavachidis 2020, 2021). Besides, the relative importance of thermal or photon desorption is still under discussion, since, according to Gamborino et al. (2019), close to the subsolar point, the Na atoms are mostly released by TD, and no more reservoir is left for PSD release. The actual temperature at which the surface transitions from retentive to emitting is a function of the binding energy of adsorbates to the surface, and if the surface is heterogeneous (e.g., consisting of different minerals), the high energy sites are filled first due to surface diffusion, leading to non-linear release with temperature (Sarantos and Tsavachidis 2021) and thus suppressing thermal desorption. Existing experiments may not have resolved these distributions as they were conducted at larger spatial scales. Thus, sensitive measurements of alkali adsorption and desorption on lunar samples at low coverages are required for improved models.

More reactive species are easier to simulate because the boundary conditions (reactions, no thermal desorption) are simpler to implement in a numerical program. Predictions for other Hermean species were presented by Wurz and Lammer (2003) using a bidimensional MC model that expanded in altitude the expected or observed exospheric densities of different species at the surface according to the energy distribution of each involved process. The Wurz et al. (2010) model update considered a more realistic surface mineralogical composition. Their results pointed out that globally the ion sputtering and MIV contributions in populating the exosphere are minor, but they could be relevant for specific refractory elements.

As MESSENGER and ground-based observations became available, some of the models of refractory species were refined, mainly in the assumptions of speed distributions of ejected atoms. Burger et al. (2014) developed a model for deriving the Ca distribution after micrometeoroid impact vaporization to be compared to the MESSENGER Ca observations, while Sarantos et al. (2011) presented an exospheric model for Mg and compared to the MESSENGER observations. They found that both these exospheres present a highly energetic component (equivalent temperature > 20,000 K) that requires a multiple step process for its generation. Plainaki et al. (2017) presented a MC model derived from the IAPS exosphere MC model for comparing the observed Ca distributions due to a possible source of micrometeoroid shower at the 2P/Encke comet trajectory crossing. This model considers for the first time after MIV the Ca release in molecular form (CaO) and shock induced photodissociation and neutralization process, as suggested by Killen (2016). The expected mapping of the impact stream onto the surface, as derived by Christou et al. (2015), was considered as input. Their results showed a well reproduced exospheric distribution, but the expected energetic Ca intensities were about 2 orders of magnitude less than observed. The study by Berezhnoy (2018) on the MIV expanded cloud shows that the resulting exospheric components from Ca bearing rocks, have higher fraction of atomic Ca than considered before (CaO 3 times more than energetic Ca).

Recently the updated IAPS MC model (Mura et al. 2007) has been used to reproduce the yearly Ca exospheric distribution considering the micrometeoroid input from Pokorný

et al. (2018) and the Berezhnoy (2018) results (Moroni et al. 2023). They found that the total exospheric Ca content is consistent with the observed one if the plume quenching temperature is less than 3750 K and not about 4000 K as considered in previous studies. In their study, relevant features are still not reproduced and they did not include the comet dust streams so that to fully describe the short and long time variabilities and the local and global features in the distributions still different assumptions have to be considered.

Predictions for a variety of refractory species (Wurz et al. 2007; Sarantos et al. 2012) cannot be tested due to the unavailability of measurements, but improved models should incorporate the non-uniform distribution of species on the surface (Prettyman et al. 2006) following those measurements of potassium which show correlation of the exosphere and surface distributions (Colaprete et al. 2016). Also, multispecies models that incorporate all existing constraints on the hydrogen and water cycle are required.

5.2 Open Issues on Exospheric Modelling

As we move forward, an improved description of gas-surface interaction, ranging from the nanoscale to the planetary scale, is required for higher fidelity models.

On the nanoscale, inputs from Molecular Dynamics (MD) simulations will provide information from first principles on the energy exchange and angular distribution of gases from smooth and rough surfaces. At the moment, such MD calculations are performed for solar wind hydrogen (Leblanc et al. 2023) and should be extended to other species discussed here (e.g., sodium). New models should include release in molecular form and consider chemical processes in the exosphere. Another effect to be considered at the atomic scale is surface diffusion between adjacent sites. Present modelling practices assume that the binding energy of an adsorbate is assigned at the time of impact and is never updated. When instead surface diffusion is permitted, the release of adsorbates at low coverages, such as experienced in most lunar regions, could be suppressed at some temperatures and enhanced at higher temperatures due to the population of sites of the highest binding energy through diffusive motion along grain boundaries (Sarrantos and Tsavachidis 2021).

On the microscale, emphasis should be placed on accounting for the effects of micro-roughness consistent due to the granular nature of regolith. The effect of small-scale shadows (<10 cm) in global models could be acknowledged through a trapping probability (Hayne et al. 2021). An additional effect to be included is that shadows at the scale of several grains can be a substantial sink for photosensitive species like sodium (Sarrantos and Tsavachidis 2020). The sputtering yields for different plasma populations as well as the angular distributions for sputtered atoms should incorporate the effect of surface micro-roughness (e.g., Cupak et al. 2021). For species of intermediate volatility and at low coverages, new models must account for the fact that release from regolith is gradual due to Knudsen diffusion into the subsurface, which decelerates desorption (e.g., Sarrantos and Tsavachidis 2021). The effect of Knudsen diffusion has been included in local simulations to estimate volatile retention at specific locations of the Moon (Schörghofer 2022; Reiss et al. 2021). However, the only global exosphere model to account for explicit diffusion into the subsurface is that of Teolis et al. (2023), and toy models approximating the effect of subsurface diffusion were proposed by Kegerreis et al. (2017). Although the effect of diffusion can be approximated in a one-layer model by adopting an effective distribution of binding sites (Sarrantos and Tsavachidis 2020), or, equivalently, by waiting times for desorption that are not exponentially distributed (e.g., log-normally distributed), solving Fick's law (Teolis et al. 2023) is the preferred solution. In the absence of experimental data, calculations with sphere packings like those of Sarrantos and Tsavachidis (2021) can be used to estimate

Knudsen and surface diffusion coefficients for global models. And finally, temperature gradients in the first few centimeters of the regolith have been adopted in simulations of volatile pumping and retention at the local scale, but not in global exosphere simulations. This is a necessary step. Calculations of these gradients based on LRO radiometer measurements exist for the Moon, and radiometer data from BepiColombo can be directly used to constrain Mercury models in the near future.

On the planetary scale, improvements to the directionality of the drivers and the effects of topography should be considered. Better description of the drivers as new inputs become available is an obvious step. Such information may include the meteoroid (Pokorný et al. 2017, 2018, 2019) and plasma directionality, the dust distribution in the interplanetary space, surface inhomogeneity and realistic compositions. New models must include large-scale topography (~1 km scale or more), which is especially important near the poles and terminators.

6 Expected Results from the Next Future Observations

In the coming years, space exploration of the inner solar system will see a golden age. In addition to the BepiColombo mission (Benkhoff et al. 2021) that will systematically observe Mercury with two spacecraft, other missions in the inner heliosphere are devoted to Sun and IMF observations, like Solar Orbiter (Müller et al. 2020) and the Parker Solar Probe (Fox et al. 2016). Moreover, the lunar exploration program, boosted by the human colonization aim, includes tens of orbital and landed missions from multiple nations and, for the first time, also by private entities. Multiple lunar landings are planned during 2023-2027 under NASA's Commercial Lunar Payload Services (CLPS) program. At the moment, flights to 11 delivery sites have been selected (Lacus Mortis, Mare Crisium, Shackleton, Reiner Gamma, Nobile, Schrödinger, Gruithuisen Domes, South Polar region, and other sites yet to be defined). The selected payloads contain neutral gas mass spectrometers, plasma spectrometers, magnetometers, and drills and sample collection for in situ analyses of volatile content. Of particular interest within the CLPS program is the Volatiles Investigating Polar Exploration Rover (VIPER) landing at Nobile Crater. VIPER will drill at several locations over a period of 100 days to determine the volatile content of sites in the south polar region as a function of depth. It carries an infrared spectrometer, a mass spectrometer, and a neutron spectrometer.

Deployment of surface instruments is also planned by human astronauts in about 2026 during the Artemis program. The ARTEMIS III Science Definition Team (SDT) Report contains several priority measurements that are relevant to exospheric processes and drivers, making it likely that some instruments with such objectives will be deployed. The Priority Goals of the SDT Report that are relevant are: 7 L-1) Understand the plasma properties near the lunar surface and how they respond to external drivers, particularly across the terminator; 7 L-2) Understand the origin of lunar surface potentials, how they evolve between sunlit and shadowed regions, and under what circumstances they pose a threat to exploration; 2E) Learn how water vapor and other volatiles are released from the surface and migrate to the poles, 5B) Heliospheric investigations using the Moon; and 7K) Understand lunar dust behaviour.

Relevant measurements from lunar orbit are expected to be conducted from the Lunar Gateway. The planned scientific payload for this station includes electron and ion spectrometers, as well as magnetometers and radiation dosimeters. Given its elliptic orbit around the Moon, the payload on the Lunar Gateway can be expected to detect lunar ions from the exosphere and surface.

Missions from other agencies include Chandrayaan 2 (ISRO), which recently refined the composition of the surface, making first distributions of global sodium on the surface available (Narendranath et al. 2022), KPL0 launched in August 2022 for characterization of the moon topography and magnetism. SELENE (KAGUYA), JAXA mission, obtained important results for the lunar environment characterization (i.e. Nagaoka et al. 2021; Yokota et al. 2020). Some major results are the identification of the reflected ions after solar wind impact onto the Moon surface (Saito et al. 2010) and the study of the interaction of plasma sheet electrons with lunar surface identified as an empty region in the electron distributions function, that was consistent with the presence of a relatively strong electric field (~ 10 mV/m) around the Moon when it is in the Earth's plasma sheet (Harada et al. 2010). Ion acceleration by the spacecraft potential and the electron beam accelerated by the potential difference between lunar surface and spacecraft were observed simultaneously when SELENE was in the Earth's magnetotail (Saito et al. 2014). These observation enable a possible way to derive the night side lunar surface potential and spacecraft potential from the observed data (Saito et al. 2014).

After the successful SELENE mission, JAXA and ISRO plan an international collaborative mission, Lunar Polar Exploration Mission (LUPEX) (<https://www.exploration.jaxa.jp/e/program/lunarpolar/>), to obtain the data on the quantity and forms of the water resources present on the Moon, to determine the feasibility of utilizing such resources for sustainable space exploration activities in the future. An Exospheric Mass Spectrometer is included in the payload.

Finally, also the Chinese space administration (CNSA) has an extensive lunar exploration program (<https://www.cnsa.gov.cn/english/index.html>). Chang'e-5 mission successfully returned lunar near-side samples. Future program includes the Chang'e-6, Chang'e-7, and Chang'e-8 missions. Chang'e-6 is poised to collect samples from the far side of the moon, marking a mission that will be the first of its kind in human history. Chang'e-7 mission will land on the lunar south pole and search for water. The final goal is to establish a scientific research station at the moon's south polar region.

This conjunction of so many important missions offers the opportunity to have unprecedented measurements of the exospheres of airless bodies, well represented by Moon and Mercury, together with the observation of the external conditions, so that, detailed investigations of the active mechanisms responsible for planet interactions with the Sun or generally with the interplanetary medium will be possible.

Improvements in ground-based observation technologies will provide a new global view of the planets at high spatial and temporal resolution to be coupled with the space observations.

The development of laboratory experiments and theoretical models and simulations related to the exosphere generation mechanisms is required for the interpretation of the expected new space data. From this point of view, fundamental new results are being achieved also thanks to the availability of powerful new computing resources. The expected outstanding results from the near future will play a crucial role in the investigation of the solar system evolution and of other planetary systems conditions.

For a better understanding of the evolution of the Sun-Earth-Moon system, a detailed investigation of the lunar exosphere, in addition to samples from the far- and near-side of the lunar surface, are of great importance. The evolutionary record of the Earth's atmosphere (e.g., Ozima et al. 2005; Terada et al. 2017; Wei et al. 2020; Lammer et al. 2022), along with traces of the young solar wind (e.g., Hodges and Hoffman 1975; Wieler et al. 1996; Marty et al. 2003) might be stored to some extent within the lunar regolith through implanted particles. During the Hadean and Archean eons, the Earth's upper atmosphere is

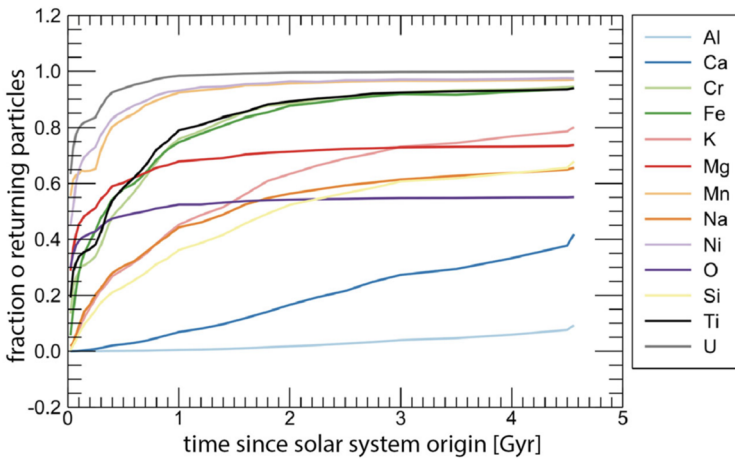


Fig. 12 The fraction of returning exospheric particles of the twelve most abundant species together with uranium that return to the Lunar surface as a function of time (Lammer et al. 2022)

thought to have been hotter and more extended than at present due to the absorption of the higher XUV flux of the young Sun (e.g., Lammer et al. 2018; Johnstone et al. 2021) indicating that atmospheric losses, i.e., the so-called ‘Earth-wind’, might have been significantly higher (Kislyakova et al. 2020). These escaping ions from Earth’s upper atmosphere were implanted into the regolith and their isotopic signatures can be measured through sampling the surface of the Moon. One can expect that these implanted particles/isotopes (N, He, Ne, Xe and Ar, etc.) will not only cause strong variations of up to 30% in the lunar regolith (Ozima et al. 2005) but these enhancements of exogenic regolith implantations should also be observed in the exosphere when they are released from the surface by various processes, as discussed in Wurz et al. (2022). As expected by Lammer et al. (2018) and Wei et al. (2020), the escape of charged particles from the Earth’s atmosphere should show a recognizable enrichment of, e.g., ^{15}N isotopes at affected areas at the nearside and farside of the lunar regolith and hence in the exosphere above these areas.

Moreover, the contribution to the lunar exosphere by micro-meteoroid bombardment was over 1000 times more relevant during early times than the contribution by sputtering (Lammer et al. 2022) while today micro-meteoroids and solar-wind ions chemically alter the lunar surface more or less in similar ways (see, e.g., Killen et al. 2012).

Additionally, to the enhanced micro-meteoroid bombardment, one can see in Fig. 12 that different return rates of various exospheric species lead to a chemical fractionation of the lunar surface over time. Due to the differing return rates of various exospheric elements, one can expect that the chemical composition of the present lunar surface does thus not reflect the surface composition after the Moons’ origin. Due to a much higher solar XUV flux, the return rates were lower billions of years ago as compared with today. From the 13 species shown in Fig. 12, uranium continuously exhibits the highest return rate due to its high mass and low ionization rate, while Al continuously exhibits the lowest return rate due to its high ionization rate and lower mass. Over time, this leads to an enrichment of uranium and a depletion of aluminium in the Lunar surface material. In a similar way, the lower return rate of K compared to U has thus led to a decrease in the lunar K/U ratio over time and might also contribute to the explanations of the low K/U ratio in the lunar surface material observed today. Thus, a detailed study of the lunar exosphere and the relevant sources and

sinks of its elements together with surface samples in the future that are collected from a large variety of different areas, can shed further light onto the evolution of the Earth-Moon system including early Earth's atmosphere and magnetosphere, the early solar wind and even the impact history of the inner Solar System. Finally, more and better data on the isotope abundances of the Moon itself of its volatile content and its related exosphere can help to separate the different lunar origin hypotheses that are discussed in Lammer et al. (2022).

Better understanding the origin of the innermost airless body in the Solar System, Mercury, is one of the greatest riddles in planetary sciences. This is specifically true since Messenger discovered that the mantle of Mercury is surprisingly volatile rich (e.g., Peplowski et al. 2011), a scientific finding that contradicted most of its previously established formation hypothesis.

The BepiColombo mission will provide unprecedented comprehensive measurements of the exosphere of Mercury. Its payload includes a mass spectrometer, an UV-Vis spectrometer, and a Na imager. The in-situ measurements of atomic and molecular exospheric densities on the day and night side, the column densities of different species and the spatial distribution of Na disk as well as the tail will be available at the same time (Milillo et al. 2020). The detailed investigation of its surface composition and magnetic field by Bepi-Colombo will help to form a clearer picture on Mercury's origin, evolution, and internal structure. These expected findings together with the discovery and investigation of so-called "Exo-Mercuries" and their statistical properties in other stellar systems by present and future ground- and space-based instrumentation such as the European Extremely Large Telescope (E-ELT), the Giant Magellan Telescope (GMT), JWST, and Ariel will tell us about their frequency and to distinguish the different formation pathways between ultra-close-in orbiting planets with silicate atmospheres and/or a stripped mantle, and planets on Mercury-like orbital distances.

Acknowledgements The authors thank ISSI for supporting the fruitful ISSI-workshop "Surface Bounded Exospheres and Interactions in the Solar System". AM is grateful to Carmelo Magnifico for the artwork of Fig. 1.

Funding Open access funding provided by Istituto Nazionale di Astrofisica (INAF) within the CRUI-CARE Agreement.

Declarations

Competing Interests The authors declare no competing interests.

Open Access This article is licensed under a Creative Commons Attribution 4.0 International License, which permits use, sharing, adaptation, distribution and reproduction in any medium or format, as long as you give appropriate credit to the original author(s) and the source, provide a link to the Creative Commons licence, and indicate if changes were made. The images or other third party material in this article are included in the article's Creative Commons licence, unless indicated otherwise in a credit line to the material. If material is not included in the article's Creative Commons licence and your intended use is not permitted by statutory regulation or exceeds the permitted use, you will need to obtain permission directly from the copyright holder. To view a copy of this licence, visit <http://creativecommons.org/licenses/by/4.0/>.

References

- Allegrini F, Dayeh MA, Desai MI, Funsten HO, Fuselier SA, Janzen PH, McComas DJ, Möbius E, Reisenfeld DB, Rodríguez M DF, Schwadron N, Wurz P (2013) Lunar energetic neutral atom (ENA) spectra measured by the interstellar boundary explorer (IBEX). *Planet Space Sci* 85:232–242. <https://doi.org/10.1016/j.pss.2013.06.014>

- Anderson KA, Lin RP, McGuire RE, McCoy JE (1975) Measurement of lunar and planetary magnetic fields by reflection of low energy electrons. *Space Sci Instrum* 1:439–470
- Anderson BJ et al (2011) The global magnetic field of Mercury from MESSENGER orbital observations. *Science* 333:1859. <https://doi.org/10.1126/science.1211001>
- Baumgardner J, Luetgten S, Schmidt C, Mayyasi M, Smith S, Martinis C, Wroten J, Moore L, Mendillo M (2021) Long-term observations and physical processes in the Moon's extended sodium tail. *J Geophys Res* 126(3):e2020JE006671. <https://doi.org/10.1029/2020JE006671>
- Benkhoff J et al (2021) BepiColombo – mission overview and science goals. *Space Sci Rev* 217:90. <https://doi.org/10.1007/s11214-021-00861-4>
- Benna M, Mahaffy PR, Halekas JS, Elphic RC, Delory GT (2015) Variability of helium, neon, and argon in the lunar exosphere as observed by the LADEE NMS instrument. *Geophys Res Lett* 42(10):3723–3729. <https://doi.org/10.1002/2015GL064120>
- Benna M, Hurley DM, Stubbs TJ, Mahaffy PR, Elphic RC (2019) Lunar soil hydration constrained by exospheric water liberated by meteoroid impacts. *Nat Geosci* 12:333–338. <https://doi.org/10.1038/s41561-019-0345-3>
- Benson J, Freeman JW, Hills HK (1975) The lunar terminator ionosphere. In: Proc of the 6th Lunar and planetary science conference proceedings, vol 6, pp 3013–3021
- Berezhnoy AA (2013) Chemistry of impact events on the Moon. *Icarus* 226(1):205–211. <https://doi.org/10.1016/j.icarus.2013.05.030>
- Berezhnoy AA (2018) Chemistry of impact events on Mercury. *Icarus* 300:210–222. <https://doi.org/10.1016/j.icarus.2017.08.034>
- Bernatowicz TJ, Podosek FA (1991) Argon adsorption and the lunar atmosphere. In: Proc. Lunar Planet. Sci. Conf., vol 21, pp 307–313
- Bida TA, Killen RM (2017) Observations of the minor species Al and Fe in Mercury's exosphere. *Icarus* 289:227–238. <https://doi.org/10.1016/j.icarus.2016.10.019>
- Bida T, Killen RM, Morgan TH (2000) Discovery of Ca in the atmosphere of Mercury. *Nature* 404:159–161. <https://doi.org/10.1038/35004521>
- Bjorkholm P, Golub L, Gorenstein P (1973) Detection of a nonuniform distribution of polonium-210 on the Moon with the Apollo 16 alpha particle spectrometer. *Science* 180(4089):957–959
- Broadfoot AL, Kumar S, Belton MJS, McElroy MB (1974) Mercury's atmosphere from Mariner 10: preliminary results. *Science* 185(4146):166–169
- Broadfoot AL, Shemansky DE, Kumar S (1976) Mariner 10: Mercury atmosphere. *Geophys Res Lett* 3(10):577–580
- Bruevich EA, Yakunina GV (2017) Flare activity of the sun and variations in its UV emission during cycle 24. *Astrophysics* 60(3). <https://doi.org/10.1007/s10511-017-9492-7>
- Burger MH, Killen RM, McClintock WE, Merkel AW, Vervack RJ, Cassidy TA, Sarantos M (2014) Seasonal variability in Mercury's dayside calcium exosphere. *Icarus* 238:51–58. <https://doi.org/10.1016/j.icarus.2014.04.049>
- Carrillo-Sánchez JD, Nesvorný D, Pokorný P, Janches D, Plane JMC (2016) Sources of cosmic dust in the Earth's atmosphere. *Geophys Res Lett* 43(23):11979. <https://doi.org/10.1002/2016GL071697>
- Cassidy TA, Merkel AW, Burger MH, Sarantos M, Killen RM, McClintock WE, Vervack RJ (2015) Mercury's seasonal sodium exosphere: MESSENGER orbital observations. *Icarus* 248:547–559. <https://doi.org/10.1016/j.icarus.2014.10.037>
- Cassidy TA, McClintock WE, Killen RM, Sarantos M, Merkel AW, Vervack RJ, Burger MH (2016) A cold-pole enhancement in Mercury's sodium exosphere. *Geophys Res Lett* 43:11,121–11,128. <https://doi.org/10.1002/2016GL071071>
- Chabot NL, Shread EE, Harmon JK (2018) Investigating Mercury's south polar deposits: Arecibo radar observations and high-resolution determination of illumination conditions. *J Geophys Res, Planets* 123:666–681. <https://doi.org/10.1002/2017JE005500>
- Chowdhury AR et al (2020) Imaging infrared spectrometer onboard Chandrayaan-2 orbiter. *Curr Sci* 118(3):368–375. <https://doi.org/10.18520/cs/v118/i3/368-375>
- Christou AA, Killen RM, Burger MH (2015) The meteoroid stream of comet encke at Mercury: implications for Mercury surface, space ENvironment, GEOchemistry, and ranging observations of the exosphere. *Geophys Res Lett* 42:7311–7318. <https://doi.org/10.1002/2015GL065361>
- Cintala MJ (1992) Impact-induced thermal effects in the lunar and Mercurian regoliths. *J Geophys Res* 97:947–973. <https://doi.org/10.1029/91JE02207>
- Colaprete A et al (2010) Detection of water in the LCROSS ejecta plume. *Science* 330:463. <https://doi.org/10.1126/science.1186986>
- Colaprete A, Sarantos M, Wooden DH, Stubbs TJ, Cook AM, Shirley M (2016) How surface composition and meteoroid impacts mediate sodium and potassium in the lunar exosphere. *Science* 351(6270):249–252. <https://doi.org/10.1126/science.aad2380>

- Cremonese G et al (2020) SIMBIO-SYS: cameras and spectrometer for the BepiColombo mission. *Space Sci Rev* 216(5):1–78. <https://doi.org/10.1007/s11214-020-00704-8>
- Crider DH, Vondrak RR (2000) The solar wind as a possible source of lunar polar hydrogen deposits. *J Geophys Res, Planets* 105(E11):26773–26782
- Crider DH, Vondrak RR (2003) Space weathering effects on lunar cold trap deposits. *J Geophys Res, Planets* 108(E7)
- Cupak C, Szabo PS, Biber H, Stadlmayr R, Grave C, Fellingner M, Brötznner J, Wilhelm RA, Möller W, Mutzke A, Moro MV, Aumayr F (2021) Sputter yields of rough surfaces: importance of the mean surface inclination angle from nano- to microscopic rough regimes. *Appl Surf Sci* 570:151204. <https://doi.org/10.1016/j.apsusc.2021.151204>
- Dandouras I et al (2023) Space plasma physics science opportunities for the lunar orbital platform - gateway. *Front. Astron. Space Sci.*, vol 10. <https://doi.org/10.3389/fspas.2023.1120302>
- Das TP, Thampi SV, Dhanya MB, Naik N, Sreelatha P, Pradeepkumar P et al (2020) Chandra's atmospheric composition explorer-2 onboard Chandrayaan-2 to study the lunar neutral exosphere. *Curr Sci* 118:202–209. <https://doi.org/10.18520/cs/v118/i2/202-209>
- Dhanya MB et al (2021) Argon-40 in lunar exosphere: observations from Chace-2 on Chandrayaan-2 orbiter. *Geophys Res Lett* 48(20):e2021GL094970. <https://doi.org/10.1029/2021GL094970>
- Delcourt DC, Grimald S, Leblanc F, Berthelier J-J, Millilo A, Mura A (2003) A quantitative model of planetary Na+ contribution to Mercury's magnetosphere. *Ann Geophys* 21:1723–1736. <https://doi.org/10.5194/angeo-21-1723-2003>
- Denevi BW, Robinson MS, Boyd AK, Sato H, Hapke BW, Hawke BR (2014) Characterization of space weathering from lunar reconnaissance orbiter camera ultraviolet observations of the Moon. *J Geophys Res, Planets* 119(5):976–997. <https://doi.org/10.1002/2013JE004527>
- Dewey RM, Slavin JA, Raines JM, Azari AR, Sun W (2020) MESSENGER observations of flow braking and flux pileup of dipolarizations in Mercury's magnetotail: evidence for current wedge formation. *J Geophys Res* 125:e2020JA028112. <https://doi.org/10.1029/2020JA028112>
- Dong C, Wang L, Hakim A, Bhattacharjee A, Slavin JA, DiBraccio GA, Germaschewski K (2019) Global ten-moment multifluid simulations of the solar wind interaction with Mercury: from the planetary conducting core to the dynamic magnetosphere. *Geophys Res Lett* 46:11588–11596. <https://doi.org/10.1029/2019GL083180>
- Farrell WM, Hurley DM, Poston MJ, Hayne PO, Szalay JR, McLain JL (2019) The young age of the LAMP-observed frost in lunar polar cold traps. *Geophys Res Lett* 46(15):8680–8688. <https://doi.org/10.1029/2019GL083158>
- Fatemi S, Lue C, Holmstrom M, Poppe AR, Wieser M, Barabash S, Delory GT (2015) Solar wind plasma interaction with Gerasimovich lunar magnetic anomaly. *J Geophys Res Space Phys* 120:4719–4735. <https://doi.org/10.1002/2015JA021027>
- Feldman WC, Maurice S, Binder AB, Barraclough BL, Elphic RC, Lawrence DJ (1998) Fluxes of fast and epithermal neutrons from lunar prospector: evidence for water ice at the lunar poles. *Science* 281:1496–1500. <https://doi.org/10.1126/science.281.5382.1496>
- Feldman PD, Hurley DM, Retherford KD, Gladstone GR, Stern SA, Pryor W, Parker JW, Kaufmann DE, Davis MW, Versteeg MH (2012) Temporal variability of lunar exospheric helium during January 2012 from LRO/LAMP. *Icarus* 221(2):854–858. <https://doi.org/10.1016/j.icarus.2012.09.015>
- Fentzke JT, Janches D (2008) A semi-empirical model of the contribution from sporadic meteoroid sources on the meteor input function observed at arcibo. *J Geophys Res Space Phys* 113:A03304. <https://doi.org/10.1029/2007JA012531>
- Fox NJ, Velli MC, Bale SD et al (2016) The solar probe plus mission: humanity's first visit to our star. *Space Sci Rev* 204:7. <https://doi.org/10.1007/s11214-015-0211-6>
- Fray N, Schmitt B (2009) Sublimation of ices of astrophysical interest: a bibliographic review. *Planet Space Sci* 57:2053–2080. <https://doi.org/10.1016/j.pss.2009.09.011>
- Futaana Y, Barabash S, Wieser M, Lue C, Wurz P, Vorburger A, Bhardwaj A, Asamura K (2013) Remote energetic neutral atom imaging of electric potential over a lunar magnetic anomaly. *Geophys Res Lett* 40:262–266. <https://doi.org/10.1002/grl.50135>
- Gamborino D, Vorburger A, Wurz P (2019) Mercury's sodium exosphere: an ab initio calculation to interpret MESSENGER observations. *Ann Geophys* 37:455–470. <https://doi.org/10.5194/angeo-2018-109>
- Gorenstein P, Bjorkholm P (1973) Detection of Radon emanation from the crater Aristarchus by the Apollo 15 alpha particle spectrometer. *Science* 179(4075):792–794
- Grava C, Chaufray J-Y, Retherford KD, Gladstone GR, Greathouse TK, Hurley DM, Hodges RR, Bayless AJ, Cook JC, Stern SA (2015) Lunar exospheric argon modeling. *Icarus* 255:135–147. <https://doi.org/10.1016/j.icarus.2014.09.029>
- Grava C, Killen RM, Benna M, Berezhnoy AA, Halekas JS, Leblanc F, Nishino MN, Plainaki C, Raines JM, Sarantos M, Teolis BD, Tucker OJ, Vervack RJ, Vorburger A (2021a) Volatiles and refractories in

- surface-bounded exospheres in the inner Solar System. *Space Sci Rev* 217:61. <https://doi.org/10.1007/s11214-021-00833-8>
- Grava C, Hurlley DM, Feldman PD, Retherford KD, Greathouse TK, Pryor WR, Gladstone GR, Halekas JS, Mandt K, Wyrick DY, Davis MW, Egan AF, Kaufman DE, Versteeg M, Stern SA (2021b) LRO/LAMP observations of the lunar helium exosphere: constraints on thermal accommodation and outgassing rate. *Mon Not R Astron Soc* 501(3):4438–4451. <https://doi.org/10.1093/mnras/staa3884>
- Halekas JA, Angelopoulos V, Sibeck DG, Khurana KK, Russell CT, Delory GT et al (2011) First results from ARTEMIS, a new two-spacecraft lunar mission: counter-streaming plasma populations in the lunar wake. *Space Sci Rev* 165(1–4):93–107. <https://doi.org/10.1007/s11214-010-9738-8>
- Halekas JA, Poppe AR, Delory GT, Sarantos M, Farrell WM, Angelopoulos V, McFadden JP (2012) Lunar pickup ions observed by ARTEMIS: spatial and temporal distribution and constraints on species and source locations. *J Geophys Res, Planets* 117:E06006. <https://doi.org/10.1029/2012JE004107>
- Halekas JS, Benna M, Mahaffy PR, Elphic RC, Poppe AR, Delory GT (2015) Detections of lunar exospheric ions by the LADEE neutral mass spectrometer. *Geophys Res Lett* 42(13):5162–5169. <https://doi.org/10.1002/2015gl064746>
- Harada Y et al (2010) Interaction between terrestrial plasma sheet electrons and the lunar surface: SELENE (Kaguya) observations. *Geophys Res Lett* 37(19):L10202. <https://doi.org/10.1029/2010GL044574>
- Harada Y, Futaana Y, Barabash S, Wieser M, Wurz P, Bhardwaj A, Asamura K, Saito Y, Yokota S, Tsunakawa H, Machida S (2014a) Backscattered energetic neutral atoms from the Moon in the Earth's plasma sheet observed by Chandrayaan-1/subkeV atom reflecting analyser instrument. *J Geophys Res* 119(5):3573–3584. <https://doi.org/10.1002/2013JA019682>
- Harada Y, Halekas JS, Poppe AR, Kurita S, McFadden JP (2014b) Extended lunar precursor regions: electron wave interaction. *J Geophys Res* 119:9160–9173. <https://doi.org/10.1002/2014JA020618>
- Hayne PO et al (2015) Evidence for exposed water in the Moon's south polar regions from lunar reconnaissance orbiter ultraviolet albedo and temperature measurements. *Icarus* 255:58–69
- Hayne PO, Aharonson O, Schorghofer N (2021) Micro cold traps on the Moon. *Nat Astron* 5(2):169–175
- Hiesinger H et al (2020) Studying the composition and mineralogy of the Hermean surface with the Mercury Radiometer and Thermal Infrared Spectrometer (MERTIS) for the BepiColombo mission: an update. *Space Sci Rev* 216. <https://doi.org/10.1007/s11214-020-00732-4>
- Hinton FL, Tausch DR (1964) Variation of the lunar atmosphere with the strength of the solar wind. *J Geophys Res* 69(7):1341–1347
- Hodges RR Jr (1973a) Differential equation for exospheric lateral transportation and its application to terrestrial hydrogen. *J Geophys Res* 78(31):7340–7346
- Hodges RR Jr (1973b) Helium and hydrogen in the lunar atmosphere. *J Geophys Res* 78(34):8055–8064
- Hodges RR (1975) Formation of the lunar atmosphere. *Moon* 14(1):139
- Hodges RR Jr (1977) Release of radiogenic gases from the moon. *Phys Earth Planet Inter* 14(3):282–288. [https://doi.org/10.1016/0031-9201\(77\)90178-9](https://doi.org/10.1016/0031-9201(77)90178-9)
- Hodges RR Jr (1980) Methods for Monte Carlo simulation of the exospheres of the Moon and Mercury. *J Geophys Res Space Phys* 85(A1):164–170
- Hodges RR Jr (2016) Methane in the lunar exosphere: implications for solar wind carbon escape. *Geophys Res Lett* 43(13):6742–6748. <https://doi.org/10.1002/2016GL068994>
- Hodges RR Jr (2018) Semiannual oscillation of the lunar exosphere: implications for water and polar ice. *Geophys Res Lett* 45(15):7409–7416. <https://doi.org/10.1029/2018GL077745>
- Hodges RR Jr, Johnson FS (1968) Lateral transport in planetary exospheres. *J Geophys Res* 73(23):7307–7317
- Hodges RR Jr, Hoffman JH (1975) Implications of atmospheric ^{40}Ar escape on the interior structure of the Moon. In: Proceedings of the 6th lunar science conference, pp 3039–3047
- Hodges RR Jr, Mahaffy PR (2016) Synodic and semiannual oscillations of argon-40 in the lunar exosphere. *Geophys Res Lett* 43(1):22–27. <https://doi.org/10.1002/2015GL067293>
- Hoffman JH, Hodges RR Jr, Johnson FS, Evans DE (1973) Lunar atmospheric 1414 composition results from Apollo 17. In: Proc of the 4th Lunar and Planetary Science Conference
- Hood LL, Williams CR (1989) The lunar swirls: distribution and possible origins. In: Proc 19th Lunar and Planetary Science Conference (A89-36486 15-91). LPI, Houston, pp 99–113
- Huntent DM, Morgan TM, Shemansky DM (1988) The Mercury atmosphere. In: *Mercury* (A89-43751 19-91). University of Arizona Press, Tucson, pp 562–612
- Hurlley DM, Cook JC, Benna M, Halekas JS, Feldman PD, Retherford KD, Hodges RR, Grava C, Mahaffy P, Gladstone GR, Greathouse T, Kaufmann DE, Elphic RC, Stern AS (2016) Understanding temporal and spatial variability of the lunar helium atmosphere using simultaneous observations from LRO, LADEE, and ARTEMIS. *Icarus* 273:45–52. <https://doi.org/10.1016/j.icarus.2015.09.011>
- Imber SM, Slavin JA (2017) MESSENGER observations of magnetotail loading and unloading: implications for substorms at Mercury. *J Geophys Res Space Phys* 122:11,402–11,412. <https://doi.org/10.1002/2017JA024332>

- Janches D, Pokorny P, Sarantos M, Szalay JR, Horanyi M, Nesvorný D (2018) Constraining the ratio of micrometeoroids from short- and long-period comets at 1 AU from LADEE observations of the lunar dust cloud. *Geophys Res Lett* 45:1713–1722. <https://doi.org/10.1002/2017GL076065>
- Janches D, Apostolos C, Berezhnoy AA, Cremonese G, Hirai T, Horanyi M, Jasinski JM, Sarantos M (2021) Meteoroids as one of the sources for exosphere formation on airless bodies in the inner solar system. *Space Sci Rev* 217:50. <https://doi.org/10.1007/s11214-021-00827-6>
- Jasinski JM, Regoli LH, Cassidy TA et al (2020) A transient enhancement of Mercury's exosphere at extremely high altitudes inferred from pickup ions. *Nat Commun* 11:4350. <https://doi.org/10.1038/s41467-020-18220-2>
- Jia X, Slavin JA, Gombosi TI, Daldorff LKS, Toth G, van der Holst B (2015) Global MHD simulations of Mercury's magnetosphere with coupled planetary interior: induction effect of the planetary conducting core on the global interaction. *J Geophys Res Space Phys* 120:4763–4775. <https://doi.org/10.1002/2015JA021143>
- Jia X, Slavin JA, Poh G, DiBraccio GA, Toth G, Chen Y et al (2019) MESSENGER observations and global simulations of highly compressed magnetosphere events at Mercury. *J Geophys Res* 124:229–247. <https://doi.org/10.1029/2018JA026166>
- Johnstone CP, Lammer H, Kislyakova K, Scherf M, Güdel M (2021) The young Sun's XUV-activity as a constraint for lower CO₂-limits in the Earth's Archean atmosphere. *Earth Planet Sci Lett* 576:117197. <https://doi.org/10.1016/j.epsl.2021.117197>
- Kallio E, Dyadechkin S, Wurz P, Khodachenko M (2019) Space weathering on the Moon: farside-nearside solar wind precipitation asymmetry. *Planet Space Sci* 166:9–22. <https://doi.org/10.1016/j.pss.2018.07.013>
- Kameda S, Yoshikawa I, Kagitani M, Okano S (2009) Interplanetary dust distribution and temporal variability of Mercury's atmospheric Na. *Geophys Res Lett* 36(15):L15201. <https://doi.org/10.1029/2009GL039036>
- Kegerreis JA, Eke VR, Massey RJ, Beaumont SK, Elphic RC, Teodoro LF (2017) Evidence for a localized source of the argon in the lunar exosphere. *J Geophys Res, Planets* 122(10):2163–2181
- Killen RM (2016) Pathways for energization of Ca in Mercury's exosphere. *Icarus* 268:32–36. <https://doi.org/10.1016/j.icarus.2015.12.035>
- Killen RM, Ip W-H (1999) The surface-bounded atmospheres of Mercury and the Moon. *Rev Geophys* 37:361–406. <https://doi.org/10.1029/1999RG900001>
- Killen RM, Hahn JM (2015) Impact vaporization as a possible source of Mercury's calcium exosphere. *Icarus* 250:230–237. <https://doi.org/10.1016/j.icarus.2014.11.035>
- Killen RM, Potter AE, Reiff P, Sarantos M, Jackson BV, Hick P, Giles B (2001) Evidence for space weather at Mercury. *J Geophys Res* 106:20509–20525. <https://doi.org/10.1029/2000JE001401>
- Killen RM, Sarantos M, Potter AE, Reiff P (2004) Source rates and ion recycling rates for Na and K in Mercury's atmosphere. *Icarus* 171:1–19. <https://doi.org/10.1016/j.icarus.2004.04.007>
- Killen RM, Cremonese G, Lammer H, Orsini S, Potter AE, Sprague AL, Wurz P, Khodachenko M, Lichtenegger HIM, Milillo A, Mura A (2007) Processes that promote and deplete the exosphere of Mercury. *Space Sci Rev* 132:433–509. <https://doi.org/10.1007/s11214-007-9232-0>
- Killen RM, Hurley DM, Farrell WM (2012) The effect on the lunar exosphere of a coronal mass ejection passage. *J Geophys Res* 117:e27837. <https://doi.org/10.1029/2011JE004011>
- Killen RM, Williams DR, Park J, Tucker OJ, Kim S-J (2019) The lunar neon exosphere seen in LACE data. *Icarus* 329:246–250. <https://doi.org/10.1016/j.icarus.2019.04.018>
- Kislyakova KG, Johnstone CP, Scherf M, Holmström M, Alexeev II, Lammer H, Khodachenko ML, Güdel M (2020) Evolution of the Earth's polar outflow from mid-Archean to present. *J Geophys Res* 125(8):e27837. <https://doi.org/10.1029/2020JA027837>
- Kobayashi M et al (2020) Mercury Dust Monitor (MDM) onboard the Mio Orbiter of the BepiColombo mission. *Space Sci Rev* 216. <https://doi.org/10.1007/s11214-020-00775-7>
- Koschny D, Grün E (2001) Impacts into ice-silicate mixtures: ejecta mass and size distributions. *Icarus* 154:402–411. <https://doi.org/10.1006/icar.2001.6708>
- Krüger H, Strub P, Srama R, Kobayashi M, Arai T, Kimura H, Hirai T, Moragas-Klostermeyer G, Altobelli N, Sterken VJ, Agarwal J, Sommer M, Grün E (2019) Modelling DESTINY+ interplanetary and interstellar dust measurements en route to the active asteroid (3200) Phaethon. *Planet Space Sci* 172:22–42. <https://doi.org/10.1016/j.pss.2019.04.005>
- Lammer H, Zerkle AL, Gebauer S, Tosi N, Noack L, Scherf M, Pilat-Lohinger E, Güdel M, Grenfell JL, Godolt M, Nikolau A (2018) Origin and evolution of the atmospheres of early Venus, Earth and Mars. *Astron Astrophys Rev* 26:2. <https://doi.org/10.1007/s00159-018-0108-y>
- Lammer H, Scherf M, Ito Y, Mura A, Vorbürger A, Guenther E, Wurz P, Erkaev NV, Odert P (2022) The exosphere as a boundary: origin and evolution of airless bodies in the inner solar system and beyond including planets with silicate atmospheres. *Space Sci Rev* 218:15. <https://doi.org/10.1007/s11214-022-00876-5>

- Lawrence DJ (2017) A tale of two poles: toward understanding the presence, distribution, and origin of volatiles at the polar regions of the Moon and Mercury. *J Geophys Res, Planets* 122(1):21–52. <https://doi.org/10.1002/2016JE005167>
- Lawson SL, Feldman WC, Lawrence DJ, Moore KR, Elphic RC, Belian RD, Maurice S (2005) Recent outgassing from the lunar surface: the lunar prospector alpha particle spectrometer. *J Geophys Res, Planets* 110(E9):E09009. <https://doi.org/10.1029/2005JE002433>
- Leblanc F, Johnson RE (2003) Mercury's sodium exosphere. *Icarus* 164:261–281. [https://doi.org/10.1016/S0019-1035\(03\)00147-7](https://doi.org/10.1016/S0019-1035(03)00147-7)
- Leblanc F, Johnson RE (2010) Mercury exosphere. I. Global circulation model of its sodium component. *Icarus* 209:280–300. <https://doi.org/10.1016/j.icarus.2010.04.020>
- Leblanc F, Doressoundiram A (2011) Mercury exosphere: II. The sodium/potassium ratio. *Icarus* 211:10–20. <https://doi.org/10.1016/j.icarus.2010.09.004>
- Leblanc F, Doressoundiram A, Schneider N, Mangano V, Lopez-Ariste A, Lemen C, Gelly B, Barbieri C, Cremonese G (2008) High latitude peaks in Mercury's sodium exosphere: spectral signature using THEMIS solar telescope. *Geophys Res Lett* 35:L18204. <https://doi.org/10.1029/2008GL035322>
- Leblanc F, Schmidt C, Mangano V, Mura A, Cremonese G, Raines JM, Jasinski JM, Sarantos M, Milillo A, Killen RM, Massetti S, Cassidy T, Vervack RJ Jr, Kameda S, Capria MT, Horanyi M, Janches D, Berezhnoy A, Christou A, Hirai T, Lierle P, Morgenthaler J (2022) Comparative Na and K Mercury and Moon exospheres. *Space Sci Rev* 218:2. <https://doi.org/10.1007/s11214-022-00871>
- Leblanc F, Deborde R, Tramontina D, Bringa E, Chaufray JY, Aizawa S, Modolo R, Morrissey L, Woodson A, Verkercke S, Dukes C (2023) On the origins of backscattered solar wind energetic neutral hydrogen from the Moon and Mercury. *Planet Space Sci* 229:105660. <https://doi.org/10.1016/j.pss.2023.105660>
- Li S et al (2018) Direct evidence of surface exposed water ice in the lunar polar regions. *Proc Natl Acad Sci* 115:8907–8912
- Lindsay ST, James MK, Bunce EJ, Imbera SM, Korth H, Martindale A, Yeoman TK (2016) MESSENGER X-ray observations of magnetosphere–ray interaction on the nightside of Mercury. *Planet Space Sci* 125:72–79. <https://doi.org/10.1016/j.pss.2016.03.005>
- Lucey PG et al (2022) Volatile interactions with the lunar surface. *Geochem* 82:125858
- Lue C, Futaana Y, Barabash S, Wieser M, Holmström M, Bhardwaj A, Dhanya MB, Wurz P (2011) Strong influence of lunar crustal fields on the solar wind flow. *Geophys Res Lett* 38:L03202. <https://doi.org/10.1029/2010GL046215>
- Mall U, Kirsch E, Cierpka K, Wilken B, Söding A, Neubauer F et al (1998) Direct observation of lunar pick-up ions near the Moon. *Geophys Res Lett* 25(20):3799–3802. <https://doi.org/10.1029/1998GL900003>
- Mangano V, Milillo A, Mura A, Orsini S, De Angelis E, Di Lellis P, Wurz AM (2007) The contribution of impulsive meteoritic impact vaporization to the Hermean exosphere. *Planet Space Sci* 55(11):1541–1556. <https://doi.org/10.1016/j.pss.2006.10.008>
- Mangano V, Leblanc F, Barbieri C, Massetti S, Milillo A, Cremonese G, Grava C (2009) Detection of a southern peak in Mercury's sodium exosphere with the TNG in 2005. *Icarus* 201:424–431. <https://doi.org/10.1016/j.icarus.2009.01.016>
- Mangano V, Massetti S, Milillo A, Plainaki C, Orsini S, Rispoli R, Leblanc F (2015) THEMIS Na exosphere observations of Mercury and their correlation with in-situ magnetic field measurements by MESSENGER. *Planet Space Sci* 115:102–109. <https://doi.org/10.1016/j.pss.2015.04.001>
- Marty B, Hashizume K, Chaussidon M, Wieler R (2003) Nitrogen isotopes on the Moon: archives of the solar and planetary contributions to the inner solar system. *Space Sci Rev* 106:175–196. <https://doi.org/10.1023/A:1024689721371>
- Massetti S, Mangano V, Milillo A, Mura A, Orsini S, Plainiki C (2017) Short-term observations of double peaked Na emission from Mercury's exosphere. *Geophys Res Lett*. <https://doi.org/10.1002/2017GL073090>
- McClintock WE, Vervack RJ Jr, Todd Bradley E, Killen RM, Sprague AL, Izenberg NR (2008) Mercury's exosphere: observations MESSENGER's first Mercury flyby. *Science* 321:92–94. <https://doi.org/10.1126/science.1159467>
- McComas DJ, Allegrini F, Bochsler P, Frisch P, Funsten HO, Gruntman M et al (2009) Lunar backscatter and neutralization of the solar wind: first observations of neutral atoms from the Moon. *Geophys Res Lett* 36(12):L12104. <https://doi.org/10.1029/2009GL038794>
- McComas DJ et al (2018) Interstellar mapping and acceleration probe (IMAP): a new NASA mission. *Space Sci Rev* 214(8):116. <https://doi.org/10.1007/s11214-018-0550-1>
- Merkel AW, Vervack RJ Jr, Cassidy TA, Killen RM, McClintock WE, Nittler LR, Burger MH (2018) Evidence connecting Mercury's Mg exosphere to its Magnesium-rich Surface Terrane. *Geophys Res Lett* 45(14). <https://doi.org/10.1029/2018GL078407>
- Milillo A, Wurz P, Orsini S, Delcourt D, Kallio E, Killen RM et al (2005) Surface-exosphere-magnetosphere system of Mercury. *Space Sci Rev* 117(3–4):397–443. <https://doi.org/10.1007/s11214-005-3593-z>

- Milillo A, Fujimoto M, Murakami G, Benkhoff J, Zender J, Aizawa S et al (2020) Investigating Mercury's environment with the two-spacecraft BepiColombo mission. *Space Sci Rev* 216(5):1–78. <https://doi.org/10.1007/s11214-020-00712-8>
- Milillo A, Mangano V, Massetti S, Mura A, Plainaki C, Alberti T, Ippolito A, Ivanovski S, Aronica A, De Angelis E, Kazakov A, Noschese R, Orsini S, Rispoli R, Sordini R, Vertolli N (2021) Exospheric Na distributions along the Mercury orbit with the THEMIS telescope. *Icarus* 355:114179. <https://doi.org/10.1016/j.icarus.2020.114179>
- Milligan RO (2015) Extreme ultra-violet spectroscopy of the lower solar atmosphere during solar flares. *Sol Phys* 290:3399–3423. <https://doi.org/10.1007/s11207-015-0748-2>
- Moroni M, Mura A, Milillo A, Plainaki C, Mangano V, Alberti T, Andre N, Aronica A, De Angelis E, Del Moro D, Kazakov A, Massetti S, Orsini S, Rispoli R, Sordini R (2023) Micro-meteoroids impact vaporization as source for Ca and CaO exosphere along Mercury's orbit. *Icarus* 401. <https://doi.org/10.1016/j.icarus.2023.115616>
- Müller D, St. Cyr OC, Zouganelis I et al (2020) The solar orbiter mission. Science overview. *Astron Astrophys* 642:A1. <https://doi.org/10.1051/0004-6361/202038467>
- Mura A, Milillo A, Orsini S, Massetti S (2007) Numerical and analytical model of Mercury's exosphere: dependence on surface and external conditions. *Planet Space Sci* 55:1569–1583. <https://doi.org/10.1016/j.pss.2006.11.028>
- Mura A, Wurz P, Lichtenegger HIM, Schleicher H, Lammer H, Delcourt D, Milillo A, Orsini S, Massetti S, Khodachenko ML (2009) The sodium exosphere of Mercury: comparison between observations during Mercury's transit and model results. *Icarus* 200:1–11. <https://doi.org/10.1016/j.icarus.2008.11.014>
- Mura A, Plainaki C, Milillo A, Mangano V, Alberti T, Massetti S, Orsini S, Moroni M, De Angelis S, Rispoli R, Sordini R (2023) The yearly variability of the sodium exosphere of Mercury: a toy model. *Icarus* 394:115441. <https://doi.org/10.1016/j.icarus.2023.115441>
- Nagaoka H, Ohtake M, Shirai N, Karouji Y, Kayama M, Daket Y, Hasebe N, Ebihara M (2021) Investigation of the source region of the lunar-meteorite group with the remote sensing datasets: implication for the origin of mare volcanism in mare imbrium. *Icarus* 371:114690. <https://doi.org/10.1016/j.icarus.2021.114690>
- Narendranath S, Pillai NS, Tadepalli SP, Sarantos M, Vadodariya K, Sarwade A, Radhakrishna V, Tyagi A (2022) Sodium distribution on the Moon. *Astrophys J Lett* 937:L23. <https://doi.org/10.3847/2041-8213/ac905a>
- Nénon Q et al (2019) Phobos surface sputtering as inferred from MAVEN ion observations. *J Geophys Res* 124:3385–3401. <https://doi.org/10.1029/2019JE006197>
- Ness NF, Behannon KW, Lepping RP, Whang YC (1975) The magnetic field of Mercury, 1. *J Geophys Res* 80:2708. <https://doi.org/10.1029/JA080i019p02708>
- Ness NF, Behannon KW, Lepping RP, Whang YC (1976) Observations of Mercury's magnetic field. *Icarus* 28(4):479–488. [https://doi.org/10.1016/0019-1035\(76\)90121-4](https://doi.org/10.1016/0019-1035(76)90121-4)
- Nishino MN, Harada Y, Saito Y, Tsunakawa H, Takahashi F, Yokota S, Matsushima M, Shibuya H, Shimizu H (2017) Kaguya observations of the lunar wake in the terrestrial foreshock: surface potential change by bow-shock reflected ions. *Icarus* 293:45–51. <https://doi.org/10.1016/j.icarus.2017.04.005>
- Orsini S, Mangano V, Mura A, Turrini D, Massetti S, Milillo A, Plainaki C (2014) The influence of space environment on the evolution of Mercury. *Icarus* 239:281–290. <https://doi.org/10.1016/j.icarus.2014.05.031>
- Orsini S, Mangano V, Milillo A, Plainaki C, Mura A, Raines JM, De Angelis E, Rispoli R, Lazzarotto F, Aronica A (2018) Mercury sodium exospheric emission as a proxy for solar perturbations transit. *Sci Rep* 8:928. <https://doi.org/10.1038/s41598-018-19163-x>
- Øieroset M, Lin RP, Phan TD, Larson DE, Bale SD (2002) Evidence for Electron Acceleration up to 300 keV in the Magnetic Reconnection Diffusion Region of Earth's Magnetotail. *Phys Rev Lett* 89:195001. <https://doi.org/10.1103/PhysRevLett.89.195001>
- Orsini S et al (2021) SERENA: particle instrument suite for Sun-Mercury interaction insights on-board Bepi-Colombo. *Space Sci Rev* 217(11):1–107. <https://doi.org/10.1007/s11214-020-00787-3>
- Ozguc A, Kilcik AK, Sarp V, Yeşilyaprak H, Pektaş R (2021) Periodic variation of solar flare index for the last solar cycle (Cycle 24), SI predictions of solar activity cycle and its association with geomagnetic activity. *Adv Astron* 5391091. <https://doi.org/10.1155/2021/5391091>
- Ozima M, Seki K, Terada N, Miura YN, Podosek FA, Shinagawa H (2005) Terrestrial nitrogen and noble gases in lunar soils. *Nature* 436:655–659. <https://doi.org/10.1038/nature03929>
- Paige DA, Wood SE, Vasavada AR (1992) The thermal stability of water ice at the poles of Mercury. *Science* 258(5082):643–646. <https://doi.org/10.1126/science.258.5082.643>
- Paige DA, Siegler MA, Zhang JA et al (2010) Diviner lunar radiometer observations of cold traps in the Moon's south polar region. *Science* 330(6003):479–482. <https://doi.org/10.1126/science.1187726>

- Peplowski PN, Evans LG, Hauck SA, McCoy TJ, Boynton WV, Gillis-Davis JJ, Ebel DS, Goldsten JO, Hamara DK, Lawrence DJ, McNutt RL, Nittler LR, Solomon SC, Rhodes EA, Sprague AL, Starr RD, Stockstill-Cahill KR (2011) Radioactive elements on Mercury's surface from MESSENGER: implications for the planet's formation and evolution. *Science* 333(6051):1850. <https://doi.org/10.1126/science.1211576>
- Peplowski PN, Evans LG, Stockstill-Cahill KR, Lawrence DJ, Goldsten JO, McCoy TJ, Nittler LR, Solomon SC, Sprague AL, Starr RD, Weider SZ (2014) Enhanced sodium abundance in Mercury's North polar region revealed by the MESSENGER gamma-ray spectrometer. *Icarus* 228:86–95. <https://doi.org/10.1016/j.icarus.2013.09.007>
- Pieters CM, Noble SK (2016) Space weathering on airless bodies. *J Geophys Res* 121:1865–1884. <https://doi.org/10.1002/2016JE005128>
- Plainaki C, Milillo A, Orsini S, Mura A, DeAngelis E, DiLellis AM, Dotto E, Livi S, Mangano V, Massetti S, Palumbo ME (2009) Space weathering on near-Earth objects investigated by neutral-particle detection. *Planet Space Sci* 57:384–392. <https://doi.org/10.1016/j.pss.2008.12.002>
- Plainaki C, Mura A, Milillo A, Orsini S, Livi S, Mangano V, Massetti S, Rispoli R, DeAngelis E (2017) Investigation of the possible effects of comet Encke's meteoroid stream on the Ca exosphere of Mercury. *J Geophys Res Planet* 122:1217–1226. <https://doi.org/10.1002/2017JE005304>
- Platz T, Nathues A, Schorghofer N et al (2017) Surface water-ice deposits in the northern shadowed regions of Ceres. *Nat Astron* 1:0007. <https://doi.org/10.1038/s41550-016-0007>
- Pokorný P, Sarantos M, Janches D (2017) Reconciling the dawn/dusk asymmetry in Mercury's exosphere with the micrometeoroid impact directionality. *Astrophys J Lett* 842:L17. <https://doi.org/10.3847/2041-8213/aa775d>
- Pokorný P, Sarantos M, Janches D (2018) A comprehensive model of the meteoroid environment around Mercury. *Astrophys J* 863(1):31. <https://doi.org/10.3847/1538-4357/aa051>
- Pokorný P, Janches D, Sarantos M, Szalay JR, Horányi M, Nesvorný D, Kuchner MJ (2019) Meteoroids at the Moon: orbital properties, surface vaporization, and impact ejecta production. *J Geophys Res, Planets* 124:752–778. <https://doi.org/10.1029/2018JE005912>
- Poppe AR (2016) An improved model for interplanetary dust fluxes in the outer Solar System. *Icarus* 264:369–386. <https://doi.org/10.1016/j.icarus.2015.10.001>
- Poppe AR, Sarantos M, Halekas JS, Delory GT, Saito Y, Nishino M (2014) Anisotropic solar wind sputtering of the lunar surface induced by crustal magnetic anomalies. *Geophys Res Lett* 41(14):4865–4872
- Poppe AR, Samad R, Halekas JS, Sarantos M, Delory GT, Farrell WM et al (2012) ARTEMIS observations of lunar pick-up ions in the terrestrial magnetotail. *Geophys Res Lett* 39(L17104). <https://doi.org/10.1029/2012gl052909>
- Poppe AR, Halekas JS, Szalay JR, Horányi M, Levin Z, Kempf S (2016) LADEE/LDEX observations of lunar pickup ion distribution and variability. *Geophys Res Lett* 43(7):3069–3077. <https://doi.org/10.1002/2016gl068393>
- Poppe AR, Halekas JS, Harada Y (2022) A comprehensive model for pickup ion formation at the Moon. *J Geophys Res, Planets* 127(10):e2022JE007422. <https://doi.org/10.1029/2022JE007422>
- Potter AE, Killen RM (2008) Observations of the sodium tail of Mercury. *Icarus* 194(1):1–12. <https://doi.org/10.1016/j.icarus.2007.09.023>
- Potter AE, Morgan TH (1985) Discovery of sodium in the atmosphere of Mercury. *Science* 229:651–653
- Potter AE, Morgan TH (1986) Potassium in the atmosphere of Mercury. *Icarus* 67:336–340
- Potter AE, Morgan TH (1988) Discovery of sodium and potassium vapor in the atmosphere of the Moon. *Science* 241:675–680. <https://doi.org/10.1126/science.229.4714.651>
- Potter AE, Morgan TH (1990) Evidence for magnetospheric effects on the sodium atmosphere of Mercury. *Science* 248:835. <https://doi.org/10.1126/science.248.4957.835>
- Potter AE, Morgan TH (1997) Sodium and potassium atmospheres of Mercury. *Planet Space Sci* 45(1):95–100. [https://doi.org/10.1016/S0032-0633\(96\)00100-6](https://doi.org/10.1016/S0032-0633(96)00100-6)
- Potter AE, Killen RM, Morgan TH (1999) Rapid changes in the sodium exosphere of Mercury. *Planet Space Sci* 47:1441–1448. [https://doi.org/10.1016/S0032-0633\(99\)00070-7](https://doi.org/10.1016/S0032-0633(99)00070-7)
- Potter AE, Anderson CM, Killen RM, Morgan TH (2002a) Ratio of sodium to potassium in the Mercury exosphere. *J Geophys Res* 107(E6). <https://doi.org/10.1029/2000JE001493>
- Potter AE, Killen RM, Morgan TH (2002b) The sodium tail of Mercury. *Meteorit Planet Sci* 37:1165–1172
- Potter AE, Killen RM, Sarantos M (2006) Spatial distribution of sodium on Mercury. *Icarus* 181:1–12. <https://doi.org/10.1016/j.icarus.2005.10.026>
- Prettyman TH, Hagerty JJ, Elphic RC, Feldman WC, Lawrence DJ, McKinney GW, Vaniman DT (2006) Elemental composition of the lunar surface: Analysis of gamma ray spectroscopy data from Lunar Prospector. *J Geophys Res, Planets* 111(E12). <https://doi.org/10.1029/2005JE002656>
- Raines JM, Gershman DJ, Zurbuchen TH, Sarantos M, Slavin JA, Gilbert JA et al (2013) Distribution and compositional variations of plasma ions in Mercury's space environment: the first three Mercury years


- of MESSENGER observations. *J Geophys Res Space Phys* 118(4):1604–1619. <https://doi.org/10.1029/2012JA018073>
- Raines JM, DiBraccio GA, Cassidy TA, Delcourt DC, Fujimoto M, Jia X, Mangano V, Milillo A, Sarantos M, Slavin JA, Wurz P (2015) Plasma sources in planetary magnetospheres: Mercury. *Space Sci Rev* 192(1):1–54. <https://doi.org/10.1007/s11214-015-0193-4>
- Reiss P, Warren T, Sefton-Nash E, Trautner R (2021) Dynamics of subsurface migration of water on the Moon. *J Geophys Res, Planets* 126(5):e2020JE006742
- Ribas I, Guinan EF, Güdel M, Audard M (2005) Evolution of the solar activity over time and effects on planetary atmospheres. I. High-energy irradiances (1–1700 Å). *Astrophys J* 622:680. <https://doi.org/10.1086/427977>
- Rognini E, Mura A, Capria MT, Milillo A, Zinzi A, Galluzzi V (2022) Effects of Mercury surface temperature on the sodium abundance in its exosphere. *Planet Space Sci* 212:105397. <https://doi.org/10.1016/j.pss.2021.105397>
- Rosborough SA, Oliverson RJ, Mierkiewicz EJ, Sarantos M, Robertson SD, Kurupparatchi DCP, Derr NJ, Gallant MA, Roesler FL (2019) High-resolution potassium observations of the lunar exosphere. *Geophys Res Lett* 46(12):6964–6971. <https://doi.org/10.1029/2019GL083022>
- Saito Y, Yokota S, Asamura K, Tanaka T, Nishino MN, Yamamoto T, Terakawa Y, Fujimoto M, Hasegawa H, Hayakawa H, Hirahara M, Hoshino M, Machida S, Mukai T, Nagai T, Nagatsuma T, Nakagawa T, Nakamura M, Oyama K, Sagawa E, Sasaki S, Seki K, Shinohara I, Terasawa T, Tsunakawa H, Shibuya H, Matsushima M, Shimizu H, Takahashi F (2010) In-flight performance and initial results of plasma energy angle and composition experiment (PACE) on SELENE (Kaguya). *Space Sci Rev* 154:265–303. <https://doi.org/10.1007/s11214-010-9647-x>
- Saito Y, Nishino MN, Fujimoto M, Yamamoto T, Yokota S, Tsunakawa H, Shibuya H, Matsushima M, Shimizu H, Takahashi F (2012) Simultaneous observation of the electron acceleration and ion deceleration over lunar magnetic anomalies. *Earth Planets Space* 64:83–92. <https://doi.org/10.5047/eps.2011.07.011>
- Saito Y, Nishino MN, Yokota S, Tsunakawa H, Matsushima M, Takahashi F, Shibuya H, Shimizu H (2014) Night side lunar surface potential in the Earth's magnetosphere. *Adv Space Res* 54(10):1985–1992. <https://doi.org/10.1016/j.asr.2013.05.011>
- Sarantos M, Killen RM, McClintock WE, Bradley ET, Vervack RJ Jr, Benna M, Slavin JA (2011) Limits to Mercury's magnesium exosphere from MESSENGER second flyby observations. *Planet Space Sci* 59(15):1992–2003. <https://doi.org/10.1016/j.pss.2011.05.002>
- Sarantos M, Killen RM, Sharma AS, Slavin JA (2008) Influence of plasma ions on source rates for the lunar exosphere during passage through the Earth's magnetosphere. *Geophys Res Lett* 35:L04105. <https://doi.org/10.1029/2007GL032310>
- Sarantos M, Killen RM, Glenar DA, Benna M, Stubbs TJ (2012) Metallic species, oxygen and silicon in the lunar exosphere: Upper limits and prospects for LADEE measurements. *J Geophys Res Space Phys* 117(A3). <https://doi.org/10.1029/2011JA017044>
- Sarantos M, Tsavachidis S (2020) The boundary of alkali surface boundary exospheres of Mercury and the Moon. *Geophys Res Lett* 47:e2020GL088930. <https://doi.org/10.1029/2020GL088930>
- Sarantos M, Tsavachidis S (2021) Lags in desorption of lunar volatiles. *Astrophys J Lett* 919(2):L14. <https://doi.org/10.3847/2041-8213/ac205b>
- Schaible MJ, Baragiola RA (2014) Hydrogen implantation in silicates: the role of solar wind in SiOH bond formation on the surfaces of airless bodies in space. *J Geophys Res, Planets* 119:2017. <https://doi.org/10.1002/2014JE004650>
- Schläppli B, Altwegg K, Wurz P (2008) Asteroid exosphere: a simulation for the Rosetta flyby targets (2867) Steins and (21) Lutetia. *Icarus* 195:674–685. <https://doi.org/10.1016/j.icarus.2007.12.021>
- Schleicher H, Wiedemann G, Wöhl H, Berkefeld T, Soltan D (2004) Detection of neutral sodium above Mercury during the transit on 2003 May 7. *Astron Astrophys* 425:1119–1124. <https://doi.org/10.1051/0004-6361:20040477>
- Schmidt CA (2013) Monte Carlo modeling of north-south asymmetries in Mercury's sodium exosphere. *J Geophys Res Space Phys* 118:4564. <https://doi.org/10.1002/jgra.50396>
- Schmidt CA, Baumgardner J, Mendillo M, Wilson JK (2012) Escape rates and variability constraints for high-energy sodium sources at Mercury. *J Geophys Res Space Phys* 117:A03301. <https://doi.org/10.1029/2011JA017217>
- Schörghofer N, Benna M, Berezhnoy AA, Greenhagen B, Jones BM, Li S, Orlando TM, Prem P, Tucker OJ, Wöhler C (2021) Water group exospheres and surface interactions on the Moon, Mercury, and Ceres. *Space Sci Rev* 217:74. <https://doi.org/10.1007/s11214-021-00846-3>
- Schörghofer N (2022) Gradual sequestration of water at lunar polar conditions due to temperature cycles. *Astrophys J Lett* 927(2):L34. <https://doi.org/10.3847/2041-8213/ac5a48>

- Seki K, Hirahara M, Terasawa T, Shinohara I, Mukai T, Saito Y, Machida S, Yamamoto T, Kokubun S (1996) Coexistence of Earth-origin O⁺ and solar wind-origin H⁺/He⁺⁺ in the distant magnetotail. *Geophys Res Lett* 23(9):985–988. <https://doi.org/10.1029/96GL00768>
- Shemansky DE (1988) Revised atmospheric species abundances at Mercury: the debacle of bad g values. *The Mercury Messenger*, LPI Contribution No. 2712
- Slade MA, Butler BJ, Muhleman DO (1992) Mercury radar imaging: evidence for polar ice. *Science* 258:635–639. <https://doi.org/10.1126/science.258.5082.635>
- Slavin JA, Middleton HR, Raines JM, Jia X, Zhong J, Sun W-J, Livi S, Imber SM, Poh G-K, Akhavan-Tafti M, Jasinski JM, DiBraccio GA, Dong C, Dewey RM, Mays ML (2019) MESSENGER observations of disappearing dayside magnetosphere events at Mercury. *J Geophys Res Space Phys* 124:6613–6635. <https://doi.org/10.1029/2019JA026892>
- Slavin JA, Imber SM, Raines JM (2021) A dungey cycle in the life of Mercury's magnetosphere, Chap. 34. In: Maggiolo R et al (eds) *Magnetospheres in the solar system*. Geophysical monograph, vol 259. AGU, pp 535–556. <https://doi.org/10.1002/9781119815624.ch34>
- Smolka A, Nikolić D, Gscheidle C, Reiss P (2023) Coupled H, H₂, OH, and H₂O lunar exosphere simulation framework and impacts of conversion reactions. *Icarus* 397:115508
- Smyth WH (1986) Nature and variability of Mercury's sodium atmosphere. *Nature* 323:696–699
- Smyth WH, Marconi ML (1995) Theoretical overview and modeling of the sodium and potassium atmospheres of Mercury. *Astrophys J* 441:839–864. <https://doi.org/10.1086/175407>
- Sprague AL, Kozłowski RWH, Hunten DM, Schneider NM, Domingue DL, Wells WK, Schmitt W, Fink U (1997) Distribution and abundance of sodium in Mercury's atmosphere, 1985–1988. *Icarus* 129:506–527. <https://doi.org/10.1006/icar.1997.5784>
- Sridharan R, Ahmed SM, Das TP, Sreelatha P, Padeepkumar P, Naik N, Supriya G (2010) The sunlit lunar atmosphere: a comprehensive study by Chace on the moon impact probe of Chandrayaan-1. *Planet Space Sci* 58:1567–1577. <https://doi.org/10.1016/j.pss.2010.07.027>
- Stern SA (1999) The lunar atmosphere: history, status, current problems, and context. *Rev Geophys* 37(4):453–491. <https://doi.org/10.1029/1999RG900005>
- Stern SA, Cook JC, Chaufray JY, Feldman PD, Gladstone GR, Retherford KD (2013) Lunar atmospheric H₂ detections by the LAMP UV spectrograph on the lunar reconnaissance orbiter. *Icarus* 226(2):1210–1213. <https://doi.org/10.1016/j.icarus.2013.07.011>
- Sun W, Slavin JA, Milillo A, Orsini S, Jia X, Raines JM, Livi S, Jasinski JM, Dewey RM, Fu S, Zhao J, Zong Q-G, Saito Y, Li C (2022) MESSENGER observations of planetary ion enhancements at Mercury's northern magnetospheric cusp during flux transfer event showers. *J Geophys Res Space Phys* 127:e2022JA030280. <https://doi.org/10.1029/2022JA030280>
- Szabo S, Poppe AR, Biber H, Mutzke A, Pichler J, Jäggi N, Galli A, Wurz P, Aumayr F (2022a) Deducing lunar regolith porosity from energetic neutral atom emission. *Geophys Res Lett* 49:e2022GL101232. <https://doi.org/10.1029/2022GL101232>
- Szabo PS, Cupak C, Biber H, Jäggi N, Galli A, Wurz P, Aumayr F (2022b) A theoretical model for the sputtering of rough surfaces. *Surfaces and Interfaces* 30. <https://doi.org/10.1016/j.surfin.2022.101924>
- Szalay JR, Horányi M (2016) Lunar meteoritic gardening rate derived from in situ LADEE/LDEX measurements. *Geophys Res Lett* 43(10):4893. <https://doi.org/10.1002/2016GL069148>
- Tanaka T, Saito Y, Yokota S, Asamura K, Nishino MN, Tsunakawa H et al (2009) First in situ observation of the moon-originating ions in the Earth's magnetosphere by MAP-PACE on SELENE (KAGUYA). *Geophys Res Lett* 36(22):L22106. <https://doi.org/10.1029/2009gl040682>
- Teolis B, Sarantos M, Schorghofer N, Jones B, Grava C, Mura A, Prem P, Greenhagen B, Capria MT, Cremonese G, Lucchetti A, Galluzzi V (2023) Surface exospheric interactions. *Space Sci Rev* 219:4. <https://doi.org/10.1007/s11214-023-00951-5>
- Terada K, Yokota S, Saito Y, Kitamura N, Asamura K, Nishino MN (2017) Biogenic oxygen from Earth transported to the Moon by a wind of magnetospheric ions. *Nat Astron* 1:0026. <https://doi.org/10.1038/s41550-016-0026>
- Troshichev O, Kokubun S, Kamide Y, Nishida A, Mukai T, Yamamoto T (1999) Convection in the distant magnetotail under extremely quiet and weakly disturbed conditions. *J Geophys Res* 104(A5):10249–10264. <https://doi.org/10.1029/1998JA900141>
- Tucker OJ, Farrell WM, Killen RM, Hurley DM (2019) Solar wind implantation into the lunar regolith: Monte Carlo simulations of H retention in a surface with defects and the H₂ exosphere. *J Geophys Res, Planets* 124:278–293. <https://doi.org/10.1029/2018JE005805>
- Vervack RJ Jr, Killen RM, McClintock WE, Merkel AW, Burger MH, Cassidy TA, Sarantos M, Cassidy TA (2016) New discoveries from MESSENGER and insights into Mercury's exosphere. *Geophys Res Lett* 43:11,545–11,551. <https://doi.org/10.1002/2016GL071284>
- Vorburger A, Wurz P, Barabash S, Wieser M, Futaana Y, Holmström M, Bhardwaj A, Asamura K (2012) Energetic neutral atom observations of magnetic anomalies on the lunar surface. *J Geophys Res* 117:A07208. <https://doi.org/10.1029/2012JA017553>

- Vorburger A, Wurz P, Barabash S, Wieser M, Futaana Y, Lue C, Holmström M, Bhardwaj A, Dhanya MB, Asamura K (2013) Energetic neutral atom imaging of the lunar surface. *J Geophys Res* 118(7):3937–3945. <https://doi.org/10.1002/jgra.50337>
- Vorburger A, Wurz P, Barabash S, Futaana Y, Wieser M, Bhardwaj A, Dhanya MB, Asamura K (2016) Transport of solar wind plasma onto the lunar nightside surface. *Geophys Res Lett* 43:10586–10594. <https://doi.org/10.1002/2016GL071094>
- Yokota S, Saito Y, Asamura K, Tanaka T, Nishino MN, Tsunakawa H et al (2009) First direct detection of ions originating from the Moon by MAP-PACE IMA onboard SELENE (KAGUYA). *Geophys Res Lett* 36:L11201. <https://doi.org/10.1029/2009gl038185>
- Yokota S et al (2020) KAGUYA observation of global emissions of indigenous carbon ions from the Moon. *Sci Adv* 6:19. <https://doi.org/10.1126/sciadv.aba1050>
- Wang X-D, Zong QG, Wang JS, Cui J, Reme H, Dandouras I et al (2011) Detection of $m/q = 2$ pickup ions in the plasma environment of the Moon: the trace of exospheric. *Geophys Res Lett* 38(L14204). <https://doi.org/10.1029/2011gl047488>
- Wang HZ et al (2021) Energetic neutral atom distribution on the lunar surface and its relationship with solar wind conditions. *Astrophys J Lett* 922:L41. <https://doi.org/10.3847/2041-8213/ac34f3>
- Watson K, Murray BC, Brown H (1961) The behavior of volatiles on the lunar surface. *J Geophys Res* 66:3033–3045
- Wei Y et al (2020) Implantation of Earth's atmospheric ions into the nearside and farside lunar soil: implications to geodynamo evolution. *Geophys Res Lett* 47:e2019GL086208. <https://doi.org/10.1029/2019GL086208>
- Werner E, Leblanc F, Chaufray JY, Modolo R, Aizawa S, Hadid L, Baskevitch C (2022) Modeling the impact of a strong X-class solar flare on the ion composition in Mercury's magnetosphere. *Geophys Res Lett* 49:e2021GL096614. <https://doi.org/10.1029/2021GL096614>
- Wieler R, Kehm K, Meshik A et al (1996) Secular changes in the xenon and krypton abundances in the solar wind recorded in single lunar grains. *Nature* 384:46–49. <https://doi.org/10.1038/384046a0>
- Wieser M, Barabash S, Futaana Y, Holmström M, Bhardwaj A, Sridharan R, Dhanya MB, Schaufelberger A, Wurz P, Asamura K (2010) First observation of a mini-magnetosphere above a lunar magnetic anomaly using energetic neutral atoms. *Geophys Res Lett* 37:L05103. <https://doi.org/10.1029/2009GL041721>
- Winslow RM, Anderson BJ, Johnson CL, Slavin JA, Korth H et al (2013) Mercury's magnetopause and bow shock from MESSENGER magnetometer observations. *J Geophys Res Space Phys* 118:2213–2227. <https://doi.org/10.1002/jgra.50237>
- Wilson JK, Mendillo M, Spence H (2006) Magnetospheric influence on the Moon's exosphere. *J Geophys Res* 111:107207. <https://doi.org/10.1029/2005JA011364>
- Wurz P, Lammer H (2003) Monte-Carlo simulation of Mercury's exosphere. *Icarus* 164(1):1–13. [https://doi.org/10.1016/S0019-1035\(03\)00123-4](https://doi.org/10.1016/S0019-1035(03)00123-4)
- Wurz P, Rohner U, Whitby JA, Kolb C, Lammer H, Dobnikar P, Martín-Fernández JA (2007) The lunar exosphere: the sputtering contribution. *Icarus* 191(2):486–496. <https://doi.org/10.1016/j.icarus.2007.04.034>
- Wurz P, Whitby JA, Rohner U, Martín-Fernández JA, Lammer H, Kolb C (2010) Self-consistent modelling of Mercury's exosphere by sputtering, micro-meteorite impact and photon-stimulated desorption. *Planet Space Sci* 58:1599–1616. <https://doi.org/10.1016/j.pss.2010.08.003>
- Wurz P, Fatemi S, Galli A et al (2022) Particles and photons as drivers for particle release from the surfaces of the Moon and Mercury. *Space Sci Rev* 218:10. <https://doi.org/10.1007/s11214-022-00875-6>
- Wurz P, Gamborino D, Vorburger A, Raines JM (2019) Heavy ion composition of Mercury's magnetosphere. *J Geophys Res* 124:2603–2612. <https://doi.org/10.1029/2018JA026319>
- Zhou X-Z, Angelopoulos V, Poppe AR, Halekas JS (2013) ARTEMI observations of lunar pickup ions: mass constraints on ion species. *J Geophys Res* 118(9):1766–1774. <https://doi.org/10.1002/jgre.20125>
- Zurbuchen TH, Raines JM, Slavin JA, Gershman DJ, Gilbert JA, Gloeckler G et al (2011) MESSENGER observations of the spatial distribution of planetary ions near Mercury. *Science* 333(6051):1862–1865. <https://doi.org/10.1126/science.1211302>

Publisher's Note Springer Nature remains neutral with regard to jurisdictional claims in published maps and institutional affiliations.

Authors and Affiliations

Anna Milillo¹  · Menelaos Sarantos² · Cesare Grava³ · Diego Janches² · Helmut Lammer⁴ · Francois Leblanc⁵ · Norbert Schorghofer⁶ · Peter Wurz⁷ · Benjamin D. Teolis³ · Go Murakami⁸

- ✉ A. Milillo
anna.milillo@inaf.it
- M. Sarantos
menelaos.sarantos-1@nasa.gov
- C. Grava
cesare.grava@swri.org
- D. Janches
diego.janches@nasa.gov
- H. Lammer
helmut.lammer@oeaw.ac.at
- P. Wurz
peter.wurz@unibe.ch
- B.D. Teolis
bteolis@swri.edu
- G. Murakami
go@stp.isas.jaxa.jp

- ¹ Institute of Space Astrophysics and Planetology, INAF via del Fosso del Cavaliere 100, 00133, Rome, Italy
- ² NASA-Goddard Space Flight Center, Greenbelt, MD 20771, USA
- ³ SwRI, San Antonio, TX, 78230, USA
- ⁴ Austrian Academy of Sciences, Space Research Institute, Schmiedlstraße 6, 8042 Graz, Austria
- ⁵ LATMOS/CNRS, Sorbonne Université, UVSQ, IPSL, Paris, France
- ⁶ Planetary Science Institute, Tucson, AZ, USA
- ⁷ Physics Institute, University of Bern, Bern, Switzerland
- ⁸ Institute of Space and Astronautical Science, Japan Aerospace Exploration Agency, Sagami-hara, Kanagawa, Japan